CHALMERS
UNIVERSITY OF TECHNOLOGY

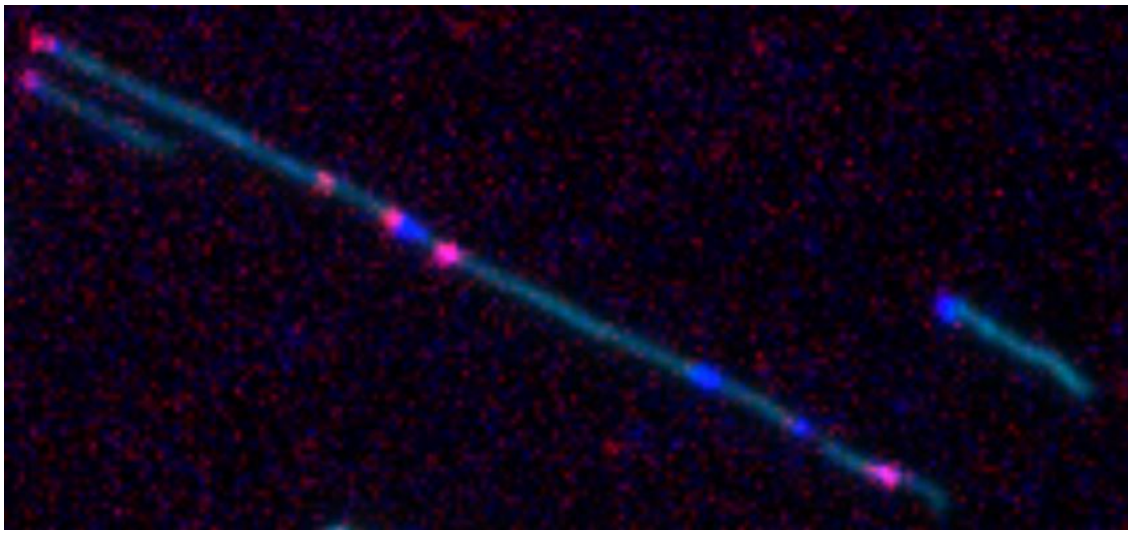

A Step Toward Personalized Cancer Treatment

Simultaneous Detection of Multiple Types of Chemotherapy-induced DNA Damage Using Single Molecule Imaging

Master's thesis in Biomedical Engineering

Ebba Foss

DEPARTMENT OF BIOLOGY AND BIOLOGICAL ENGINEERING

CHALMERS UNIVERSITY OF TECHNOLOGY
Gothenburg, Sweden 2022
www.chalmers.se

Master's thesis 2022

A Step Toward Personalized Cancer Treatment

Simultaneous Detection of Multiple Types of Chemotherapy-induced DNA Damage Using Single Molecule Imaging

EBBA FOSS

CHALMERS
UNIVERSITY OF TECHNOLOGY

Department of Biology and Biological Engineering
Division of Chemical Biology
Fredrik Westerlund Research Group
Chalmers University of Technology
Gothenburg, Sweden 2022

A Step Toward Personalized Cancer Treatment
Simultaneous Detection of Multiple Types of Chemotherapy-induced DNA Damage Using Single Molecule Imaging
EBBA FOSS

Supervisor: Obed Akwasi Aning, Division of Chemical Biology, Chalmers
Examiner: Fredrik Westerlund, Division of Chemical Biology, Chalmers

Master's Thesis 2022
Department of Biology and Biological Engineering
Division of Chemical Biology
Fredrik Westerlund Research Group
Chalmers University of Technology
SE-412 96 Gothenburg
Telephone +46 31 772 1000

Cover: An image of human DNA stained with YOYO-1 dye and visualized with fluorescence microscopy. The blue and red dots represent damage sites repaired and labelled with fluorescent nucleotides dUTP-ATTO-550 and dUTP-ATTO-647, respectively.

Typeset in LaTeX
Printed by Chalmers Reproservice
Gothenburg, Sweden 2022

A Step Toward Personalized Cancer Treatment – Simultaneous Detection of Multiple Types of Chemotherapy-induced DNA Damage Using Single Molecule Imaging

Ebba Foss
Chemical Biology Department
Chalmers University of Technology

Abstract

Chemotherapy is commonly used to treat cancer today, either alone or more commonly as part of combination therapy. Response to a certain chemotherapeutic agent is highly individual, both in terms of treatment efficacy and the extent to which healthy cells are affected. For several drugs, induced DNA damage provides the main cytotoxic effect, and a method for evaluating this damage could therefore prove a powerful tool in treatment planning. In this thesis, a single molecule imaging approach is used to assess chemotherapy-induced DNA damage, allowing visualisation of damage sites on individual DNA strands. While previous studies have focused on one damage type, or collective damage without distinction between types, a novel modification to pre-existing techniques that allows for this distinction has recently been demonstrated. In this thesis, the alkylating agent temozolomide was used to illustrate how different damage types can be distinguished with a single molecule imaging approach. This is done using repair enzymes associated with different DNA repair pathways. The repair enzymes sequentially incorporate spectrally distinct fluorescent nucleotides at the damage site which are then visualized as fluorescent spots of two different colours on individual DNA molecules. This distinction could be shown with high repeatability in terms of colour ratio. While both enzymes used separately clearly repaired the treated DNA, there appeared to be an overlap when applying them sequentially. This could suggest a problem with enzyme specificity. Further exploration of this issue is needed to verify the feasibility of single molecule imaging for the purpose of simultaneous detection of chemotherapy-induced DNA damage types.

Keywords: DNA damage; Single Molecule Imaging; Chemotherapy; Temozolomide; Simultaneous Labelling; DNA alkylation

Acknowledgements

I must firstly thank my supervisor throughout this project, Obed Akwasi Aning. Without your guidance and not-too-infrequent pep-talks, this project would not have been possible. It would also not have been possible without Fredrik Westerlund, at whose division the project was conducted. Thank you for the opportunity to do this research. A big thank you to all in Fredrik Westerlund's group as well, who have been very welcoming and helpful during this process.
Lastly, I must also thank family and friends for all their support throughout my studies. In particular Elin and Emil, with whom much of these five years were happily spent. And of course my parents; you're the best, and I couldn't have done it without you.

Ebba Foss, Gothenburg, June 2022

List of Acronyms

Below is the list of acronyms that have been used throughout this thesis:

AP	Apurinic/Apyrimidinic
APE-1	Human AP endonuclease
APTES	3-Aminopropyl-triethoxysilane
ATMS	Allyltrimethoxysilane
BER	Base Excision Repair
DMSO	Dimethylsulfoxide
DR	Direct Repair
DSB	Double-stranded Break
EDTA	Ethylenediaminetetraacetic acid
Endo III	Endonuclease III
Endo IV	Endonuclease IV
Endo VII	Endonuclease VII
Endo VIII	Endonuclease VIII
EPR	Enhanced perfusion and retention
FPG	DNA-formamidopyrimidine glycosylase
GG-NER	Global Genomic Nucleotide Excision Repair
hAAG	Human Alkyl Adenine DNA Glycosylase
HR	Homologous recombination
MGMT	O^6-methylguanine-DNA-methyltransferase
miRNA	MicroRNA
MMR	Mismatch Repair
N^7-MeG	N^7-Methylguanine
N^3-MeA	N^3-Methyladenine
NER	Nucleotide Excision Repair
NHEJ	Non-homologous End Joining
O^6-MeG	O^6-Methylguanine
PBMC	Peripheral Blood Mononuclear Cell
PBS	Phosphate Buffered Saline
rSAP	Shrimp alkaline phosphatase
SMI	Single molecule imaging
SSB	Single-stranded Break
TBE	Tris-borate EDTA
TMZ	Temozolomide
UDG	Uracil DNA glycosylase
UV	Ultraviolet

Contents

List of Figures

List of Tables

1
Introduction

Cancer is the second leading cause of death in Sweden[1], and despite progress in the field of cancer treatment, much work still remains. Chemotherapies, which aim at inducing apoptosis, and/or preventing proliferation of cancerous cells are commonly used today. There are various modes-of-action including , inhibition of DNA synthesis or the transport system of the cell. While the target is tumour cells, chemotherapeutic drugs also inevitably affect healthy cells [2], causing symptoms such as hair loss, gastro-intestinal distress, and fatigue. Sensitivity to chemotherapy varies on an individual level [3, 4] and being able to measure this in an efficient way could facilitate selection of the most suitable drug for a specific patient. This would in turn be greatly beneficial to the patients' well-being.

Many chemotherapeutic drugs are alkylating agents that readily form DNA adducts. Temozolomide (TMZ) is one such agent, whose cytotoxic effects are attributed to its tendency to methylate the O^6-position of guanine [5]. Although O^6-methylguanine (O^6-MeG) only represents around five percent of the methylations induced by TMZ, other adducts, mainly N^7-methylguanine (N^7-MeG) and N^3-methyladenine (N^3-MeA) are readily repaired by the base-excision repair system (BER)[**?**]. While these adducts represent 60-80% and 10-20% of TMZ-induced alkylations respectively, their cytotoxic effect is therefore limited. O^6-methylated guanines are often subject of direct repair (DR), in which the methyl group is removed. However, if this does not take place, the lesion is instead recognized post-replication by the mismatch repair (MMR) system due to the incorrect pairing with thymine[5]. The thymine is excised, but since O^6-MeG is not replaced, a futile repair cycle is initiated, eventually leading to double stranded DNA-breaks (DSBs).

The DNA damaging effects of chemotherapeutics have previously been evaluated using different assays, e.g., comet assays [6, 7], enzyme-linked immunosorbent assays (ELISA) [8, 9], or western blots [10, 11], the latter two of which utilize biomarkers such as DNA repair related proteins. However, these methods are typically limited to analyzing one damage type at a time [12]. DNA damage can also be evaluated directly, through visualization of individual DNA strands with single molecule imaging (SMI) [13]. This method utilizes fluorescent dyes to detect DNA molecules with a fluorescence microscope. By incorporating fluorescent nucleotides at the damage sites the induced damage can be quantified. Unlike the previously mentioned methods, this allows for higher specificity, enabling localization of single lesions on a DNA strand, rather than observing the sum of all damage on a global cellular level. Interestingly, modifications to the single strand DNA damage detection assay has now made it possible for the concurrent detection of different damage types. Torchinsky et al., employed this to simultaneously detect oxidative DNA damage

and photoproducts induced by ultra-violet (UV) radiation [14].

In the paper by Torchinsky et al., *Simultaneous Detection of Multiple DNA Damage Types by Multi-colour Fluorescent Labelling*, UV-induced photoproducts and oxidative DNA-damage was distinguished by applying repair enzymes for each damage type sequentially, together with nucleotides conjugated with one of two different fluorophores. If this method can be successfully applied to DNA from cells exposed to chemotherapy, it could prove useful in the field of personalized cancer treatment. Knowing the DNA damaging effects of chemotherapies on an individual patient level could facilitate selection of the most suitable treatment for each patient.

1.1 Thesis Statement

Understanding the effect of chemotherapeutic drugs on an individual patient level is important to ensure that patients are prescribed the safest and most effective cancer treatment possible. While the wide array of chemotherapies available can effectively treat most forms of cancer, or be combined with other therapies such as radiotherapy, they inevitably have adverse effects on healthy cells, to some extent. For several drugs, inducing DNA damage provide the main cytotoxic effect, and evaluating the induced damage in healthy cells could therefore be a powerful tool in treatment planning. While several assays for evaluating DNA damage exist, there is a distinct lack of assays in which different damage types can be differentiated. SMI is a promising candidate for detecting DNA damage that with method expansion, could allow for differentiation of damage types, whilst also providing the added benefit of observing individual DNA molecules to gain further insight on where and how damages tend to appear. This thesis, will show how this can be achieved with relatively simple modifications to the original method proposed by Torchinsky et al.

1.2 Aim

The main aim of this project was to simultaneously detect different types of DNA damage induced by the chemotherapeutic drug TMZ. Using SMI, the damage types should be visible and distinguishable. Furthermore, using these images, the extent of the different damage types induced by the drug should be quantified. For this purpose, peripheral blood mononuclear cells (PBMCs) were isolated from blood samples provided by the clinical chemistry department at Sahlgrenska University hospital and treated with varying concentrations of the chemotherapeutic drug.

The project also involved optimizing some aspects of the single-strand DNA damage detection assay by investigating which conditions for coverslip preparation and sample storage would provide adequate stretching of the DNA when performing the fluorescent imaging. This included investigating the optimal time for coverslip functionalization before imaging, the most suitable preparation method, maximum storage time of blood and DNA samples as well as appropriate storage temperature.

1.3 Limitations

Although this project intends to optimize the single-strand DNA damage detection assay to assess DNA damage induced by chemotherapeutics, the blood samples will come from healthy donors and be exposed to chemotherapeutics in a laboratory environment. As the human body is a complex system, the effect of this exposure is likely different from that of typical patient exposure. Another limitation is that only one cell type is tested. In contrast, when used for therapeutic purposes, the drug tested may affect many different cell types in the body, possibly in different ways.
Furthermore, while this project describes an assay to detect and distinguish different damage types induced by chemotherapeutics, it should be noted that evaluating the effects of the drug is not the main aim. Rather, the focus is on developing a method that could help to better understand the differential damage induced by the drug. However, being able to quantify the damage is necessary for the method to fulfill its intended purpose.

1.4 Ethical Concerns

As with all research involving human subjects or, as in this case, samples from human subjects, patient confidentiality is of utmost importance. The blood samples that were used in this research were provided by Sahlgrenska University hospital with patient consent for research purposes. The project falls under study approval by the Regional Ethical Review Board in Gothenburg (Dnr: 938-16).
The blood samples were provided with a sample ID, patient name and national ID. After relevant information was noted, all papers were discarded in a confidential waste bin. To minimize the risk of data breach the sample ID, rather than national ID, was noted.

2
Theory

To motivate the various choices made during this project, as well as to propose explanations to the acquired results, some basal information must first be established. Firstly, the phenomena on which the proposed assay is based, i.e., how DNA damage occurs, how this affects the cell as well as the repair mechanisms the cell has in place are described. To relate this information to the motivation for development of this assay, the genetic mechanisms and features of cancer are then briefly explained, together with the main modes of action of common chemotherapeutic drugs. In particular, the properties of TMZ, the drug used in this paper, are described. How DNA damage can be visualized with SMI and how this process differs from established methods is also described before lastly discussing the properties of PBMCs and their potential as a source of biomarkers.

2.1 DNA damage

DNA damage can be classified as endogenous or exogenous. Endogenous damage occurs as a result of DNA reacting with celullar compounds, such as generated reactive oxygen species, spontaneous events such as deamination, or replication errors by DNA polymerases, which naturally occur approximately every 100,000 base pairs[15]. In contrast, exogenous damages are induced by non-naturally occurring compounds such as radiation and certain chemicals[16]. Damages vary in their occurence and cytotoxicity. As a majority of human DNA is non-coding, many mutations have virtually no effect on the cell[17]. In cancerous cells these can be referred to as passenger mutations as they persist in the cell genome without having a notable impact on cell behaviour and survival[18]. Conversely, mutations in coding sections of DNA can have massive detrimental effects. Point mutations, base insertions or deletions, and recombinations are examples of events that can lead to deleterious changes in protein structure and function[19] which can ultimately cause apoptosis[20]. Apoptosis is also induced by steric changes caused by certain DNA damages[21]. Extensive conformational changes affect vital cell cycle processes such as transcription and replication. If transcription is affected, the resulting changes in protein expression can lead to activation of various apoptotic signalling molecules [21]. Inhibition of replication typically causes highly cytotoxic DSBs, which in turn lead to activation of the p53 gene. Depending on expression levels, this activation either leads to cell-cycle arrest, or activation of apoptotic factors[21]. While the cell has strategies to repair these lesions, repair may lead to other issues, such as recombinations, deletions or insertions, as will be further discussed in section 2.2.

2.1.1 DNA Methylation

The methylation of DNA is not a solely damage related process. Enzymatic DNA-methylation, generally occuring on the C^5 position of cytosine, is essential for cell survival by regulating gene expression[22]. Cancerous cells exhibit abnormal methylation patterns with both hyper- and hypomethylation having been observed [23]. Detrimental methylation can be caused by e.g. alkylating agents, such as certain chemotherapeutic drugs, a common target being N^7-guanine [24]. N^7-MeG can lead to the rise of abasic sites, also known as AP sites, i.e. sites in which a purine or pyrimidine base is removed due to hydrolysis of the N-glycosyl bond. While N^7-MeG in itself is fairly benign, AP sites are mutagenic[24]. AP sites are unstable and readily lead to single stranded breaks (SSBs)[16]. If left unrepaired, SSBs may prevent replication and transcription and possibly induce apoptosis[16]. AP sites can also lead to the formation of interstrand crosslinks as will be further discussed in section 2.1.2. DNA hydrolysis can be spontaneous or occur as part of the BER pathway, in which the base is excised by glycolases such as human alkyladenineglycosylase (hAAG)[16]. Even non-methylated bases may be spontaneously removed, although at lower rates than certain methylated bases. Guanine and adenine bases are most commonly targeted, giving them significantly higher hydrolysis rates than cytosine and thymine bases[25]. The rate of spontaneous depurination of N^7-MeG increases dramatically with temperature [24].

Another common methyl adduct is O^6-MeG, which is significantly more cytotoxic than N^7-MeG[26]. O^6-MeG is a stable lesion that therefore persists and mispairs with thymine during replication, a mismatch that leads to a futile repair cycle and consequentially DSBs[21]. Apart from their role in inducing apoptosis, repair of DSBs can have mutagenic effects[27]. In particular, homologous recombination (HR), which requires a template strand, may lead to homozygosity, increasing cancer risk if including a mutation in a key sequence[27].

2.1.2 DNA crosslinks

DNA strands can form crosslinks e.g., with proteins, other DNA strands (interstrand crosslink), or within the strand itself (intrastrand crosslink). Crosslinking can have majorly detrimental effect on the cell as it may cause structural distortions that interfere with cellular processes such as replication. This interference may ultimately lead to apoptosis if the crosslink is left unresolved[28]. Crosslinks can be induced by exogenous agents, such as bifunctional alkylating agents[29]. Bifunctional alkylating agents have two reactive sites, which can thus react with two different bases, the alkylating agent serving as the link between them. Crosslinks can also be induced by endogenous sources. AP sites, which can be formed both spontaneously and due to e.g. chemical agents, can lead to the formation of interstrand crosslinks[30]. Typically the AP sites react with guanines on the opposite strand, although the rate is dependent on their relative placement [30].

2.2 DNA repair

Mutations and replication mistakes are common enough that the human cell requires a sophisticated repair system of enzymes and co-factors to preserve viability and prevent uncontrolled growth. Together they form repair pathways to cover the vast array of DNA damages that may occur.

2.2.1 Base Excision Repair (BER) Pathway

The BER pathway refers to the repair of lesions that cause limited conformational changes, such as N^7-MeG[16]. The repair is initiated by DNA-glycolases, of which several have been identified in the human genome[31]. They are usually small and positively charged[31]. The glycolases recognize lesions with varying degrees of specificity and initiate the pathway by removing the damaged base from its deoxyribose[16]. Substrates for glycosylases include oxidated and alkylated bases[31]. hAAG is a glycosylase which recognizes alkylated bases, mainly N^7-MeG and N^3-MeA[32]. The resulting AP site is recognized by secondary enzymes, which excise the remaining deoxyribose, leaving the site free for incorporation of a new nucleotide[31]. The cytotoxicity of AP sites is postulated as an explanation for the extensive repair of the relatively harmless N^7-MeG, with the suggestion that controlled repair with BER would be preferable to spontaneous depurination[33].
Depending on the glycolase involved, the repair may follow the long- or short-patch repair pathways of the BER pathway, both of which involve Apurinic/apyrimidinic (AP) endonucleases[34]. The short-patch repair pathway, which is the dominant pathway, results in the excision of a single nucleotide. AP endonuclease 1 (APE-1) and Endonuclease IV (Endo IV) are two examples of AP endonucleases in the short-patch repair pathway, human and bacterial, respectively[35]. The long-patch pathway involves removal of two to ten nucleotides and mainly occurs in proliferating cells[34].

2.2.2 Mismatch Repair (MMR) Pathway

The MMR pathway mainly acts post-replication, correcting mismatches or insertions/deletions on the newly synthesized strand, greatly improving replication fidelity[16]. However, many proteins involved in the MMR pathway seem to serve multiple functions, including DNA damage signaling and apoptosis mediation[16]. The pathway involves a multitude of complex-forming proteins to ensure recognition of the correct strand as well as enzymes responsible for excising around the lesion site. The MMR pathway is responsible for the main cytotoxic effect of O^6-MeG as described in section 2.1.1. MMR proteins serve to correct mistakes made by polymerases during replication and as such they recognize the daughter strand as the mistake, rather than the template strand[16]. As O^6-MeG is located on the template strand, this means the actual source of the mismatch is not resolved. During subsequent replication cycles, the continued strain of this repair leads to DSBs and ultimately apoptosis[21]. Furthermore, MMR binding to DNA can promote apoptosis directly [21]. Endonuclease VII (Endo VII) is a repair enzyme isolated from bacteriophage T4

which plays a role in multiple DNA pathways, including the MMR pathway. Endo VII has the ability to recognize several mismatches, including G-T mispairings[36]. However, the substrate specificity of Endo VII is broad, and the enzyme has been shown to, among other lesions, also repair 4-way Holliday junctions[37], heteroduplex loops[36], cisplatin-induced interstrand crosslinks[38] and even AP-sites[39].

2.2.3 Nucleotide Excision Repair (NER) Pathway

The nucleotide excision repair (NER) pathway is divided into the global genome NER(GG-NER) and the transcription-coupled NER(TC-NER) pathways[16]. While the former recognizes damage in both coding and non-coding regions the latter is initiated by transcription stalling and thus only repairs damage in coding DNA regions[16]. The NER system recognizes a wide range of substrates, but is mainly involved in repairing bulky lesions which cause significant structural distortions to the DNA, such as damage induced by UV-radiation, polyaromatic hydrocarbons and certain chemotherapies [40]. In GG-NER the distortions are mainly recognized by protein factor XPC, which initiates an enzyme cascade that results in an excision of approximately 20-30 bases around the lesion site[40]. While bulky lesions make up the majority of NER substrates, some overlap in substrate affinity with BER has been reported[41][42]. Plosky et al. demonstrated how GG-NER in mammalian cells has some affinity for N^7-MeG and N^3-MeA, but not TC-NER[41]. Sensitivity to alkylating agents in yeast cells mutants suggest NER is an alternative repair pathway to methylation damage, but likely without a large impact when a functional BER pathway is present[42].

2.2.4 Double Strand Break Repair Pathways

There are two main pathways to repair double strand breaks in mammalian cells: non-homologous end joining (NHEJ) and HR[27]. These pathways are also involved in repair of interstrand crosslinks. HR relies on a template strand for accurate repair. Homology on another DNA strand, i.e. on the second copy of the affected chromosome, is identified by the RAD51 protein[43]. This can then be used as a template for joining the two fragments that resulted from the DSB together[43]. Although this pathway provides high-fidelity repair, the use of a homologous sequence as template has inherent risks[27]. If the sequence to be repaired is mutated on one chromosome, this mutation will be transferred to the other chromosome as well. If the mutation is significant, having two defective gene copies may have deleterious effects on the cell and may be involved in carcinogenesis[27]. NHEJ does not rely on a template strand and is the dominant form of DSB repair[44]. The pathway instead involves recognition of DSBs and aligning of the strands which are held in place to allow for a ligase to join the ends[44]. NHEJ also involves enzymes to perform essential end processing to allow for ligation. This is due to the strand ends not generally being compatible, as they may undergo chemical modifications or loss of bases after the break occurs[44]. The strands may therefore undergo resection and as such, the NHEJ pathway can often lead to deletions or deletions together with insertions of bases. This is however not always the case, and depending on the

nature of the break and the compatibility of the ends, NHEJ can perform repair without removal of genetic information[44]. NHEJ is also involved in improving the immune system by increasing variation in immunoglobulins and T-cell receptors[45]. Programmed DSBs are repaired by NHEJ, leading to variations which increases the number of pathogens which can be recognized by the immune system[45].

2.2.5 Direct Repair (DR)

Cells have the ability to repair certain lesions directly, without removing affected bases. In contrast to the previously discussed pathways, this form of repair involves a single enzyme, typically with very high substrate specificity. DR enzymes are known to repair alkylated DNA and certain UV-induced damages[46]. In humans, one important DR enzyme is O^6-alkylguanine-DNA-alkyltransferase (MGMT). MGMT resolves some O-alkyladducts, including O^6-MeG, by transfering the methylgroup to a cysteine residue in the active site of the enzyme [46][16]. This action permanently deactivates MGMT, which is then a target of ubiquitin-mediated protein degradation[46].

2.3 Carcinogenesis

Carcinogenesis refers to the process in which sequential genetic changes leads to tumour formation due to abnormal growth and proliferation of cells[47]. In malign tumours, i.e. cancers, tumour cells can invade surrounding tissue, migrate and form metastases at secondary locations in the body[47]. Carcinogenesis can broadly be divided into three stages: initiation, promotion, and progression[47]. All three stages involve genetic changes that drive cells toward cancer cell behaviour.
Initiation involves irreversible changes to the cell genome[47]. Initiation alone is not enough for carcinogenesis, and in fact a majority of initiation events never evolve into cancers. The affected genes may be dominant oncogenes, recessive tumour suppressor genes, or microRNA (miRNA) coding genes[48]. Oncogenes promote cell proliferation and suppress apoptosis[48]. If oncogenes are upregulated, proliferation may be increased and apoptosis inhibited. Even with a functional gene on one allele, mutations in oncogenes may lead to cancer. In contrast, tumour suppressor genes transduce growth-inhibitory signals. One functional gene copy is in this case generally enough to prevent cancer formation. While oncogenes are rarely involved in inherited cancer risk, tumor suppressor genes are more commonly so[47]. The traditional view of oncogenes as dominant and tumour suppressor genes as recessive is however somewhat simplified. Having only one functional copy of a tumour suppressor gene may still impact the cell negatively. Studies have suggested that some tumour suppressor genes are haploinsufficient, i.e., one gene copy does not provide adequate activity[49]. Dysregulation of miRNA genes has also been associated with cancer, as they in turn affect expression of tumour suppressor genes and oncogenes[48].
For cancer to develop after an initiation event, a series of cancer-promoting changes generally take place. The promotion stage involves reversible changes which in many cases are due to ligand-receptor mediated alterations in gene expression[47]. Fur-

ther genetic changes, leading to structural alterations and phenotype changes occur during the progression stage[47]. General traits include uncontrolled proliferation, increased growth rate, the ability to evade apoptosis, and drug resistance[50][51]. The high growth rate increases ATP expenditure and therefore leads to a change in metabolic activity[52]. A highly important property of tumour cells is the enhanced permeability and retention (EPR), providing potential of drug accumulation with certain drug delivery systems[53]. Furthermore, the properties of tumour cells are affected by the surrounding cell environment and factors such as stiffness and fluid pressure[54].

2.4 Chemotherapy and DNA damage

Chemotherapy is a common method for treating cancer, often in conjunction with other therapies, such as radiotherapy or surgery [55]. The effectiveness of a particular drug depends on the type of tumour present and thus suggested treatment varies with cancer type [55]. As an example, brain tumours are notoriously difficult to treat. Many chemotherapeutic agents are unable to pass the blood-brain-barrier, the blood vessel structure that prevents harmful agents from passing the epithelial cells into the brain tissue[56].
Given the underlying genetic mechanisms and properties of cancer cells, chemotherapies are usually aimed at inducing apoptosis, or inhibiting proliferation of cancerous cells[57]. Chemoterapeutic drugs are divided into broad categories based on their mechanism of action. Antimetabolites such as 5-fluorouracil and methotrexate target key metabolic processes to prevent cell proliferation[55]. Other drugs such as paclitaxel and docetaxel stabilize microtubules, preventing cytoskeletal rearrangement and by extension mitosis[55]. Chemotherapeutics can also cause apoptosis by damaging DNA or other cellular structures. Alkylating agents do so by transfering alkyl groups to nucleophiles, with the N7 position of guanine representing the majority of DNA alkylations[29]. Bifunctional alkylating agents can cause crosslinks by alkylating both DNA strands[32]. Sufficient structural distortions induce apoptosis during cell replication, due to their hindering of proper DNA replication.
TMZ is a synthetically produced alkylating agent primarily used to treat certain brain malignancies due to its ability to bypass the blood-brain barrier[58]. Administered orally, the drug has a 98 % bioavailability, but it may also be administered intravenously[58]. The cytotoxic effect of TMZ can be attributed to its ability to methylate pyrimidine and purine bases. N^7-MeG is the the most common adduct, followed by N^3-MeA, however the main cytotoxic effect arises through the methylation of O^6 guanine[5]. While only accounting for approximately 5% of all TMZ-mediated methylations, O^6-MeG is a highly mutagenic adduct[58]. While N7-MeG and N^3-MeA are readily repaired by the BER pathway, O^6-MeG is mainly repaired through DR or via the MMR pathway. Typically, MGMT converts O^6-MeG back to guanine, preventing further damage, but if this process is reduced, serious damage can occur. As mentioned in section 2.2.2 O^6-MeG mismatches with thymine during replication[21]. This mismatch is recognized by enzymes in the MMR which excise the mispaired thymine rather than the O^6-MeG. As the source of the issue is not removed, the mismatch reoccurs, leading to a futile repair cycle, and finally double

stranded DNA breaks. As such, an active MMR pathway increases the sensitivity to TMZ, while high activity of MGMT reduces the therapeutic effect[58]. As a result, these enzymes provide potential targets for increasing drug efficiency[5].

2.5 DNA damage assays

The general process of SMI is described, followed by some examples of its use to assess DNA damage. To emphasize the potential benefits of SMI, other assays commonly used to study DNA damage are briefly discussed.

2.5.1 Single Molecule Imaging (SMI)

SMI refers to a series of microscopy techniques which utilize fluorescence to image individual molecules. SMI can be used to image e.g. proteins and DNA, both within and outside cells and is therefore a powerful tool in studying biological processes and functions[59]. With the subject of this thesis in mind, SMI will mostly be discussed in regard to studying DNA molecules.
In solution, DNA is naturally in a coiled state. There are several techniques for stretching DNA, including optical tweezers, DNA manipulation with electrostatic forces and interface movement[60]. Glass functionalization, typically silanization, improves stretching of DNA by providing a positively charged surface. Due to the negative but (pH-dependent) charge of the DNA, the DNA interacts with the functionalized surface[61]. 3-Aminopropyl-triethoxysilane (APTES) and Allyltrimethoxysilane (ATMS) are two compounds that can be used to improve DNA stretching. The process also involves relative movement of DNA to the surface. This can be achieved by dipping silanized coverslips in a DNA solution[62]. As the slides are removed, the resulting air-water meniscus provides the force that causes the DNA molecules to stretch. Force can also be applied by adding a sample droplet at the edge of a silanized coverslip on a glass slide. Capillary forces will pull the liquid between the coverslip and glass slide, the DNA stretching on the coverslip as the fluid floods the interface[63].
SMI has recently emerged as a method to assess DNA damage. In a 2013 study, Lee et al visualized damage induced by UV radiation on single DNA molecules with SMI using two different approaches[13]. In the first approach, DNA was stretched and immobilized on positively charged glass slides. Irradiation of the DNA with UV induced pyrimidine dimers. Addition of pyrimidine dimer glycosylase led to DSBs which could then be seen as dark areas when adding fluorescent dye and visualizing the samples with fluorescence microscopy. The authors also used UV radiation to induce damage to DNA in solution. Fluorescent nucleotides were then used to fill the gaps that appear as a consequence of DNA repair. After labelling, the DNA was immobilized and visualized with fluorescence microscopy, the damage sites appearing as dots on the DNA strands [13]. Zirkin et al. employed a similar method using U-2 OS cells rather than pure DNA. The cells were UV-radiated or treated with hydrogen peroxide to induce damage. A cocktail of repair enzymes was used to repair lesion sites, which were then filled with fluorescent nucleotides by DNA polymerase [64]. A 2020 study by Singh et al. similarly used a repair enzyme

cocktail to assess levels of DNA damage in radiated lymphocytes[63]. Based on their results, the authors proposed a potential use of the assay to identify patients with high radiation sensitivity. In a 2021 study, Singh et al. focused on single-strand breaks induced by oxidizing chemotherapeutic agent bleomycin[12]. PBMCs were isolated from blood samples and treated with bleomycin. The induced damages were repaired with a BER enzyme cocktail. The results suggested a significant variability in bleomycin sensitivity between individuals[12].
As evidenced by the studies mentioned, SMI to detect DNA damage has typically been performed to detect a single damage type or with enzyme cocktails which give no distinction between damage types. With some modifications to the assay, Torchinsky et al., described an expansion of these methods that allow for simultaneous detection of two different damage types [14]. In the study, cells were exposed to UVC radiation, causing photoproduct formation and nucleotide oxidation. The respective repair enzymes for these lesions were then applied in sequence followed by DNA polymerase incorporating fluorescent nucleotides of spectrally distinct colours. The oxidative damage repair enzymes were applied first, which excised the affected nucleotides. DNA polymerase was then added together with nucleotides to label the damage sites with the first colour. After the first labelling the remaining fluorescent nucleotides were inactivated with a shrimp alkaline phosphatase (rSAP), preventing incorporation in subsequent steps. After repair by a second enzyme, specific for photoproducts, nucleotides conjugated with a second fluorophore were added. DNA polymerase incorporated the fluorescent nucleotides at the repaired damage sites. Using this method, the authors claim they were able to produce images of DNA strands in which the UV damage sites were distinguishable from oxidative damage sites, based on colour[14]. This method could potentially be applied to other damage types, by changing the repair enzymes used.

2.5.2 Other methods to assess DNA damage

There are various assays available for assessing DNA damage, all with their respective advantages and disadvantages. The comet assay has traditionally been used to detect DSBs at a cellular level. DNA is isolated from cells and used for electrophoresis. DNA supercoiling will normally prevent DNA from travelling through the gel. Strand breaks will allow for relaxation of the DNA and the subsequently relaxed areas form a "tail" as a result of their movement. Intact DNA will thus be seen as a well-defined circle, whereas damaged DNA will have a comet-like appearance[65]. For a more specific detection of DNA damage, the addition of repair enzymes enables evaluation of different damage types such as alkylated and oxidated bases [65]. However, this method does not allow for distinction between damage types. ELISA is an immunoassay that can be used to detect the present of some DNA damage types in samples. Due to its use of antibodies however, the method is limited by the antibodies available[66]. Furthermore, ELISA only allows screening for one damage type at a time. High performance liquid chromatography (HPLC) is a high fidelity method to detect a number of modified bases and DNA damages both in terms of location and concentration[67]. HPLC is however an expensive method that requires equipment not always available. Furthermore, it necessitates a high level of

experience for accurate results[67].

2.6 Peripheral Blood Mononuclear Cells (PBMCs)

PBMCs have been indicated as a source of biomarkers for a wide range of conditions, e.g., by looking at miRNA, DNA, or protein expression[68–70]. A 2019 review study by Mosallaei et al. concluded that PBMCs held several potential biomarkers, including mRNA expression, miRNA levels, and DNA methylation [71]. The benefits lie mainly in their high availability, and ease of acquirement[72]. Blood samples are frequently drawn in hospital settings, and with patient consent, these samples can also be used for research. The relatively low discomfort of sampling, as well as the minimal effect the small samplings have on patients, make blood an attractive source of biological tissue[72].
From whole blood, PBMCs can be extracted using centrifugation induced density gradients[73]. As the name suggests, the term encompasses mononuclear blood cells, namely lymphocytes and monocytes[73]. The majority of PBMCs are B and T cells, followed by natural killer cells and monocytes[74]. Using a hydrophilic medium such as Lymphoprep^{TM}, the PBMCs are separated from the lighter plasma and denser erythrocytes and polymorphonuclear leukocytes. While the denser components sediment through the medium, PBMCs form a lightly translucent layer on top, the buffy coat.
The use of PBMC in oncology research is vast and varied. In a 2013 study, Friso et al. identified global DNA methylation as biomarker for cancer risk using PBMCs, with significantly lower methylation in cancer patients ($p < 0.0001$) [75]. Burczynski et al. found a significant difference in PBMC profiles between healthy subjects and patients with advanced renal cell carcinoma [76]. Ma et al. demonstrated the potential of PBMC miRNA to aid early detection of lung cancer[77]. Furthermore, PBMCs have been used for several clinical trials of chemotherapeutic drugs, including everolimus and iniparib[78]. While many cytotoxic drugs affect PBMCs, it should be noted that PBMCs as a surrogate for tumour tissue has its limitations such as a difference in drug accumulation[78].
As mentioned in section 2.4, TMZ is most commonly administered orally, where it is absorbed in the gastrointestinal tract, or intravenously[58]. As such, TMZ is inevitably in contact with PBMCs. TMZ has been shown to have immunosuppressive effects, decreasing e.g. lymphocyte counts[79]. PBMCs express MGMT, although with variation both between individual and with time[80]. PBMCs displayed a decrease in MGMT expression levels after exposure to TMZ, although not correlating to the effect on MGMT expression in tumour cells[81]. It should be noted that other tissues could be affected in a way that would recommend against treatment with TMZ.

3

Materials and Methods

All experiments performed during this project were performed using different combinations of a set of general methods. These methods are presented in the approximate order they would performed during a typical experiment. The process begun with the extraction of DNA from whole blood, followed by the labelling process, imaging, and ending with analysis of the resulting images. Further details on specific experiments are described in relation to these general methods.

3.1 DNA extraction from blood samples

The process of extracting DNA from whole blood can be divided into three general steps. Firstly, the cells of interest, in this case PBMCs, were isolated. The isolated cells were then treated with the desired drug concentration and treatment duration. In this study, cells were either treated with 800 μM TMZ or left untreated. After treatment, the cells were lysed and the DNA was extracted. Throughout the experiment, pipette tips were cut when handling DNA to prevent DNA shearing.

3.1.1 PBMC Isolation

To minimize the effect of individual differences, a minimum of three blood samples from different individuals were pooled together and used. Blood was mixed based on lymphocyte count to obtain a total of 500,000 lymphocytes per treatment. The blood was mixed with an equal volume of 1X phosphate buffered saline (PBS, Gibco^{TM}). A density gradient centrifugation process was used to isolate PBMCs from the blood samples. A volume of Lymphoprep^{TM} (STEMCELL technologies) equal to that of the PBS/blood mixture was added to a 15 mL falcon tube. The PBS/blood mixture was then carefully pipetted on top of the Lymphoprep^{TM}, forming two distinct layers in the tube. The tube was centrifuged at 600 rcf for 20 minutes at room temperature. The difference in density between the blood components led to a multilayered formation in the tube, with a foggy layer of lymphocytes beneath the top layer of blood plasma. The lymphocyte layer was carefully removed and put in a clean falcon tube. The cells were then washed twice by adding approximately 3 ml of 1X PBS, centrifuging at 500 rcf for 10 minutes at room temperature and discarding the supernatant each time. The remaining pellet was then resuspended in 300 μL of RPMI-1640 (Sigma-Aldrich) per treatment. For experiments regarding the effect of time on the quality of the blood samples for the proposed assay, the entire process described above was repeated at 2-4 hour intervals, as well as once

the following day.

3.1.2 PBMC treatment

300 μL of cell suspension was added to an 1.5 μL eppendorf tube. Cells were treated with 800 μM TMZ. The TMZ stock was diluted in dimethyl sulfoxide (DMSO). As negative controls, some samples were left without treatment. The samples were incubated at 37°C in a thermal block for two hours. After incubation, 100 μL of resuspension buffer (19:1 of resuspension solution (Sigma-Aldrich) and RNAse (Sigma-Aldrich)) was prepared and added per sample. After approximately a minute, 100 μL of lysis buffer (4:1 of lysis solution (Sigma-Aldrich) and proteinase K (Sigma-Aldrich)) was added per sample. Each tube was briefly vortexed before incubating at 55 °C in a thermal block for twenty minutes. For experiments regarding the effect of time on the quality of the blood samples for the proposed assay, cells were directly resuspended and lysed without the addition of any drug or incubation.

3.1.3 DNA extraction

The GenElute^{TM} mammalian genomic DNA miniprep kit (Sigma-Aldrich) was used to extract DNA from the PBMCs. Extraction columns were prepared by placing a binding column in a collecting tube (Sigma-Aldrich). 500 μL of Column Prep solution (Sigma-Aldrich) was added per tube, before spinning the tubes for 1 minute at 12000 rcf. The flow through was discarded.
200 μL of 99.5 % ethanol was added to each tube of lysed cells which were then vortexed thoroughly for 10 seconds, ensuring a homogeneous solution. The sample solutions were then placed in the prepared columns. The tubes were spun for 1 minute at 6000 rcf. The flow through was discarded and 500 μL of washing solution (Sigma-Aldrich) was added per tube before again spinning for 1 minute at 6000 rcf. This washing process was repeated before spinning the tube empty at the same settings. The columns were placed in clean collecting tubes before adding 100 μL of elution buffer (Sigma-Aldrich) onto the filter. After five minutes, the tubes were spun for 1 minute at 6000 rcf and the columns were discarded, leaving DNA in elution buffer in the collecting tubes. The DNA concentrations were then measured using a NanoDrop® ND-1000 UV-Vis Spectrophotometer (Thermo-Fisher).

3.2 DNA labelling

The process of DNA repair and labelling is here divided into single colour and dual colour labelling. The general process is described, but enzyme additions vary and are specified in tables 3.1 and 3.2.

3.2.1 Single-colour labelling

A volume equal to 100 or 50 ng of DNA, 5 μL of 10X Cutsmart buffer (NEB), and one or more enzymes, depending on the experiment, were added to a PCR tube, adding

Milli-Q®(Millipore) water to a total volume of 50 μL. For tests relating to simultaneous detection, hAAG (NEB), Endo IV (NEB), and/or Endo VII (MCLAB) were used. For tests evaluating the effect of blood storage on basal DNA damage levels, an enzyme cocktail was used. This contained APE-1, DNA-formamidopyrimidine glycosylase (FPG), uracil DNA glycosylase (UDG), endonuclease III, (Endo III), Endo IV, and endonuclease (Endo VIII), all from NEB. Enzymes and their respective amounts added are listed for each sample type in table 3.1. The sample was incubated in a T100 thermal cycler (BioRad) at 37 °C for 1 hour. A nucleotide mix was prepared consisting of 0.5 μL each of dATP, dGTP, and dCTP (all at 100 μM, NEB), 0.13 μL of dTTP (100 μM,NEB), 12.5 μL of Aminoallyl-dUTP-ATTO-550 (10 μM, Jena Bioscience), 5 μL of 10X NEB2 buffer (NEB), 1.25U DNA polymerase, topped up with MQ to a total volume of 50 μL. 50 μL of the nucleotide mix was added to each PCR tube. The samples were then incubated at 20 °C for 1 hour in the thermal cycler. after which 2.5 μL of 0.25X ethylenediaminetetraacetic acid (EDTA, Fisher Bioreagents) was added to each tube to stop the ongoing reaction. Samples were kept at -20 °C until imaging. When testing the effect of storage and storage temperature on labelled DNA, the DNA was aliquoted and kept both at -20 °C and 4 °C.

Table 3.1: Enzymes used in single colour labelling. Amounts listed as per tube.

Sample Name	Enzymes	Purpose
Both	2.5U each of hAAG, Endo IV, 3U Endo VII	Verify colour correspondence
hAAG/Endo IV	2.5U each of hAAG, Endo IV	Verify colour correspondence
Endo VII	3U Endo VII	Verify colour correspondence
Blood storage test	2U FPG, 1.25U UDG, and 2.5U each of APE 1, Endo III, Endo IV, Endo VIII	Assess effect of blood storage time on DNA quality

3.2.2 Dual-colour labelling

50 ng of DNA, 5 μL of 10X Cutsmart buffer (NEB), and enzymes were added to a PCR tube, topped up with Milli-Q® water to a total volume of 50 μL. Table 3.2 lists the enzymes added for each type of sample produced. The samples were incubated in a thermal cycler at 37 °C for 1 hour. A nucleotide mix was prepared consisting of 0.5 μL each of dATP, dGTP, and dCTP (all at 100 μM,NEB), 0.13 μL of dTTP (100 μM, NEB), 12.5 μL of aminoallyl-dUTP-ATTO-550 (10 μM, Jena Bioscience), 5 μL of 10X NEB2 buffer (NEB), 1.25U DNA polymerase, topped up with Milli-Q® to a total volume of 50 μL. 50 μL of the nucleotide mix was added to each PCR tube. The samples were then incubated at 20 °C for 1 hour. 1U of rSAP (NEB) was added per tube. The samples were then incubated at 37 °C for 10 minutes followed by 5 minutes at 65 °C to inactive the rSAP protein before the next step.
5 μL of 10X Cutsmart buffer (NEB) and the desired enzymes were mixed and then added per tube, see table 3.2, before incubating at 37 °C for 1 hour. A second nucleotide mix was prepared consisting of 0.5 μL each of dATP, dGTP, and dCTP

(all at 100 M,μ NEB), 0.13 μL of dTTP (100 M, NEB), 12.5 μL of Aminoallyl-dUTP-ATTO-647 (10 M, Jena Bioscience), 5 μL of 10X NEB2 buffer (NEB), 1.25U T4 DNA polymerase (NEB), topped up with Milli-Q® to a total volume of 50 μL. 50 μL of the nucleotide mix was added to each PCR tube and the samples were then incubated at 20 °C for 1 hour. 2.5 μL of 0.25X EDTA was added to each tube to stop the ongoing reaction. Samples were kept at -20 °C until imaging.

Table 3.2: Enzymes used in the two repair steps of the dual colour labelling assay. Amounts listed as per tube.

Sample Name	Enzymes step 1	Enzymes step 2	Purpose
Both 2 clr	2.5U each of hAAG, Endo IV	3U Endo VII	Main assay
hAAG/Endo IV 2 clr	2.5U each of hAAG, Endo IV	No enzyme	Verify colour correspondence
Endo VII 2 clr	3U Endo VII	No enzyme	Verify colour correspondence
Blank	No enzyme	No enzyme	Assess background repair

3.3 Imaging

Labelled DNA was stretched on a silanized coverslip placed on a glass slide (Epredia) and images were taken using Zeiss Observer Z1 microscope. The entire process from silanization of the coverslips to image acquisition is described in detail below.

3.3.1 Coverslip Silanization

Glass coverslips (18x18 mm, Epredia) were placed in a coverslip rack and submerged in a mixture of acetone (99,8% HPLC-grade, Fisher Chemicals) and 1% (v/v) each of APTES (99%, Sigma-Aldrich) and ATMS (95%, Sigma-Aldrich). Depending on the experiment, silanization time varied. For the experiments regarding the effect of silanization time on the stretching of DNA molecules, coverslips were placed in freshly prepared APTES/ATMS/acetone solution. Three coverslips were removed each time at 30, 60, 90, and 120 minutes after submersion in the APTES/ATMS/acetone solution and used to image immediately. In all other cases the coverslips were submerged in the prepared solution between 1 and 24 hours. The silanization solution was then replaced with pure acetone until the coverslips were used.

3.3.2 Fluorescence Microscope Imaging

Sample preparation was done under minimum light exposure to preserve fluorescence of the samples. When using human DNA, 7 μL of labelled DNA was added to 40.4 μL of 0.5X Tris-Borate-EDTA(TBE,PanReac Applichem) buffer, cutting the pipette tip to prevent shearing of the DNA. When using lambda DNA (500 μg/mL,NEB), the DNA was first diluted 1:19 in 0.5X TBE buffer. 2 μL of this dilution was then mixed with 45.4 μL of 0.5X TBE. In both cases, 1.6 μL of YOYO-1 dye (320 nM, Invitrogen) and 1 μL of β-mercaptoethanol (BME, Sigma-Aldrich) was then added to the sample. A silanized coverslip was taken and washed with a 2:1 mixture of

Acetone and Milli-Q® water, before being dried with N_2 and placed on a clean glass slide. 3.4 μL of the prepared DNA mixture was pipetted at the edge of the coverslip, allowing capillary force to stretch the DNA on the coverslip. A 100X objective was used, placing an immersion oil (Immersol 518F, Zeiss) droplet on the objective, before adding the glass slide on top. After finding DNA molecules with the focus, images were taken in one, two or three channels for the three dyes, YOYO-1 (508 nm, exposure time 150 ms), ATTO-550 (576 nm, exposure time 1500 ms), ATTO-647 (670 nm, exposure time 1000 ms). For the experiments to study the effect of silanization time on the stretching of DNA, only the YOYO-1 channel was used, for single colour labelling the YOYO-1 and ATTO-550 channels were used, and for dual colour labelling all three channels were used. Light intensity was set at 30%. Multiple images were taken per sample for quantification to minimize the impact of random variations.

3.4 Data Analysis

Multi-channel images were split into two (for single colour labelling) or three (for dual colour labelling) channels using a MATLAB script provided by the department of Astronomy and Theoretical Physics at the University of Lund. The script converts the input format of .czi to .tif to prepare the images for analysis. The images are analyzed with another script, courtesy of the same group, where the molecules and dots corresponding to fluorescent nucleotides are recognized and assigned scores. A threshold score for molecule detection was set automatically, whereas the threshold score for dot detection was set manually. By observing the histogram of the dot score and the detected molecules on the corresponding channel, the images were divided into suitable dot scores and run in groups. The length of the detected DNA and the number of dots was recorded, from which the damage can be calculated as dots per μm, and in the case of simultaneous detection, the ratio between the two colours can be calculated. For full MATLAB settings, see appendix A.1
These values were then analysed using Graphpad Prism 9. When comparing the mean of two samples, a two-tailed t-test was used to assess statistical significance. When comparing multiple samples, a one-way ANOVA test was used instead.

4

Results and Discussion

With the aims of this study falling under two general categories, the results are presented in the same fashion. In the first section, results regarding the simultaneous detection of different lesions induced by TMZ are presented and discussed. Following this discussion, results regarding the optimization of several parameters with regard to the general SMI process are also evaluated. For all experiments where p-values where calculated, the p-values are available in appendix A.2.

4.1 Simultaneous Detection of Multiple Damage Types

With the protocol described in section 3.2.2, two different dot colours representing the incorporation of two spectrally distinct nucleotides at damage sites on the same DNA strand could be visualized. Damage was then quantified as the number of dots per μm DNA. Figure 4.1 displays example snapshots of stretched DNA molecules with dots of two different colours on the strands together with the quantified damage. Figure 4.1a1 shows examples of DNA from PBMCs treated with 800 μm TMZ while figure 4.1a2 shows examples of DNA from untreated PBMCs.
Blue dots represent dUTP-ATTO-550 nucleotides which were used to fill the gaps after repair by hAAG and Endo IV. Red dots represent dUTP-ATTO-647 nucleotides which were used to fill the gaps after repair by Endo VII. To verify reproducibility, the experiment was repeated three times. The difference in damage level for blue dots between the treated samples and untreated controls was statistically significant as shown in figure 4.1b. Albeit the difference in mean number of red dots was over three-fold higher for the treated samples, a large standard variation meant it was non-significant, also seen in figure 4.1b. A difference in damage levels between untreated samples and samples treated with TMZ was expected, in accordance with literature[58]. From this data, the fraction of the total number of dots each dot colour represents could be calculated. The fractions are presented in table A.3

Table 4.1: Fraction of total damage for dUTP-ATTO-550 and dUTP-ATTO-647. Mean of three experiments.

Treatment	ATTO-550 (Blue)	ATTO-647 (Red)
800 uM TMZ	0.65	0.35
Untreated	0.62	0.38

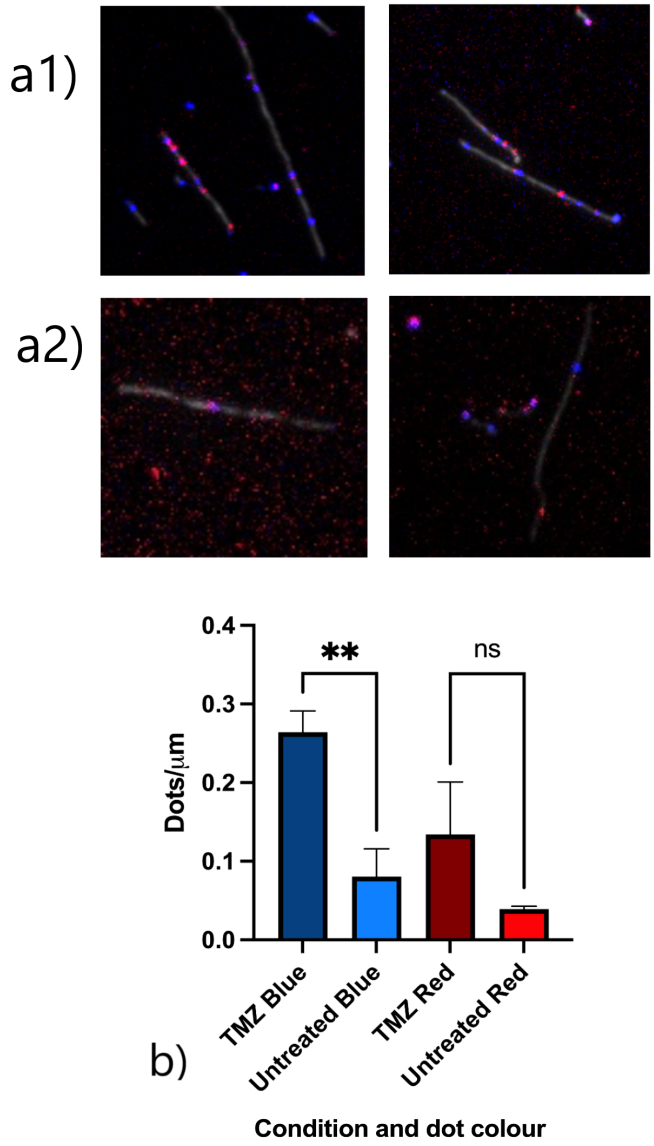

Figure 4.1: a)Images of human DNA strands stained with YOYO-1 dye and labelled with a dual colour labelling process. The DNA comes from cells incubated for two hours with either 800 μM TMZ (a1) or no treatment (a2). b) DNA damage as number of dots per μm where samples denoted 'TMZ' have been incubated with 800 μM TMZ for two hours and samples denoted 'Untreated' have been incubated for two hours without added treatment. The blue dots are from dUTP-ATTO-550, used after repair with hAAG and Endonuclease IV. The red dots are from dUTP-ATTO-647, used after repair with Endonuclease VII. Error bars represent the standard deviation of three repeats.

As can be seen in table A.3, for treated samples, blue dots stood for around 65 % of all damage, while for untreated samples, blue dots represented approximately 62 %. The proportions were not equal to the approximately 95:5 ratio of N^7-MeG/N^3-MeA to O^6-MeG mentioned in section 2.4, suggesting that the enzymes do not repair completely separate lesion types. This may be the result of overlapping enzyme specificity, or the limited specificity of many bacterial enzymes, such as Endo VII. While hAAG and Endo IV are fairly well-characterized in terms of substrate affinity and activity levels, Endo VII has not been studied as extensively. As previously mentioned, Endo VII is reported to have a broad range of substrates that suggest its involvement in several DNA repair pathways. Another possibility is that there was continued activity of hAAG/Endo IV in the later steps, which would then shift the proportion of blue and red dots. There could also possibly be some level of non-specific DNA repair by DNA polymerase. From these results it is therefore not clear what the red dots detected actually represent. It was therefore of interest to investigate whether the two different fluorescent nucleotides actually represented the enzymatic activity of the different repair steps.

4.1.1 Verification of colour-correspondence

To verify that blue dots actually corresponded to hAAG/Endo IV-repairs, and red dots to Endo VII-repairs, experiments in which only hAAG/Endo IV enzymes were used were conducted. The process described in section 3.2.2 was followed, except for the omission of Endo VII at the second repair step. The resulting damage is shown in figure 4.2. As shown in figure 4.2b, some red dots are still present even when omitting Endo VII. A possible explanation could be continued activity of the hAAG/Endo IV enzymes after the first hour of repair. Both hAAG and Endo IV require heat inactivation for 20 minutes at 65 and 85 °C respectively. The simultaneous detection assay only involves 5 minutes of incubation at 65 °C, which would therefore mean incomplete inactivation of hAAG/Endo IV. If all substrates for hAAG/Endo IV are repaired within one hour this would not lead to continued incorporation of nucleotides in the second 37 °C incubation, as the enzymes would have no lesion sites to repair. However, if this is not the case, it would be reasonable to see continued incorporation of nucleotides as the enzymes are still active.

The presence of red dots even without addition of Endo VII, suggests continued activity of hAAG/Endo IV. From the results it is however not clear if all red dots in TMZ Both are the result of the continued activity, or if they are at least partly due to Endo VII. As shown in figure 4.2b, the difference in number of red dots between TMZ Both and TMZ hAAG/Endo IV is non-significant. This could suggest that Endo VII has limited effect on the DNA, if any. To test this, two additional conditions were also investigated. The two additional conditions were included in the third repeat of the test. In the first condition Endo VII was used in the first repair step and no enzyme was added in the second repair step (TMZ Endo VII). In the second condition no enzymes were used in either repair step (TMZ Blank). All dual colour samples from this test iteration are summarized in figure 4.3. Note that three (TMZ Both, TMZ hAAG/Endo IV and Untreated Both) of the five conditions displayed

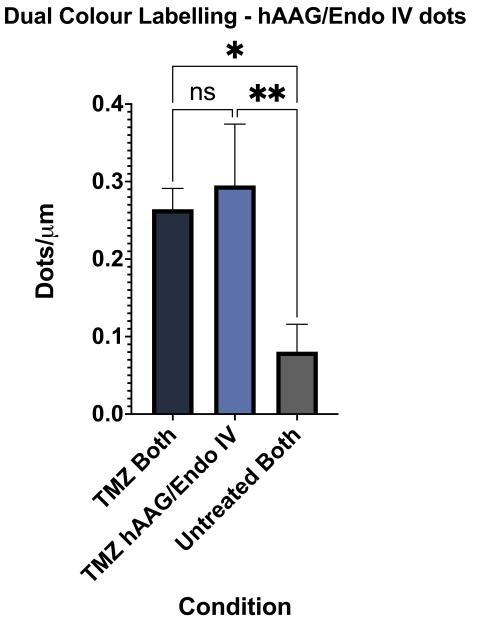

(a) Average damage recorded as the number of dUTP-ATTO-550 dots per μm DNA. Error bars represent the standard deviation of three repeats. Statistical significance calculated with a one-way ANOVA.

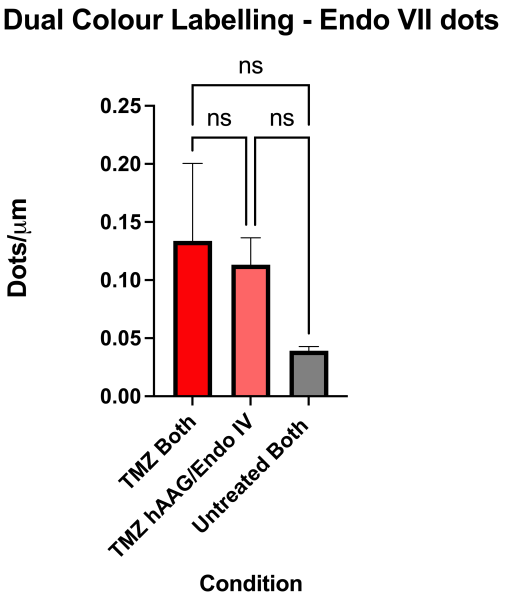

(b) Average damage recorded as the number of dUTP-ATTO-647 dots per μm DNA. Error bars represent the standard deviation of three repeats. Statistical significance calculated with a one-way ANOVA.

Figure 4.2: Average damage from three experiments. a) represents dots from the first reaction, b) represents dots from the second reaction. Samples were either labelled using hAAG and Endo IV in the first step, followed by Endo VII in the second step (TMZ Both, Untreated Both) or by using hAAG and Endo IV in the first step and no enzyme in the second step (TMZ hAAG/Endo IV)

are included in the averaged data presented in figures 4.2a and 4.2b.

As can be seen in figure 4.3, the detected damage is much lower for TMZ Blank than all other samples. This suggests that non-specific repair of TMZ-treated DNA by DNA polymerase is low. The detected damage is more than twice as high for TMZ Endo VII compared to TMZ Blank. While calculating significance with only one data point per sample is not possible, this strongly suggests Endo VII being involved in the repair of TMZ mediated DNA damage. However, the number of red dots per μm is similar for TMZ hAAG/Endo IV, TMZ Endo VII and TMZ both. This is in contrast to the number of blue dots per μm which is drastically decreased when excluding hAAG/Endo IV. It thus becomes difficult to deduce from which repair enzyme the red dots in TMZ Both result.

As previously mentioned, 65 °C for five minutes is not enough to inactivate hAAG/Endo IV, and as such there may be a continued repair process during the second 37 °C incubation, if one hour is insufficient for the hAAG and Endo IV enzymes to repair all relevant lesions. This could easily be investigated by extending the incubation

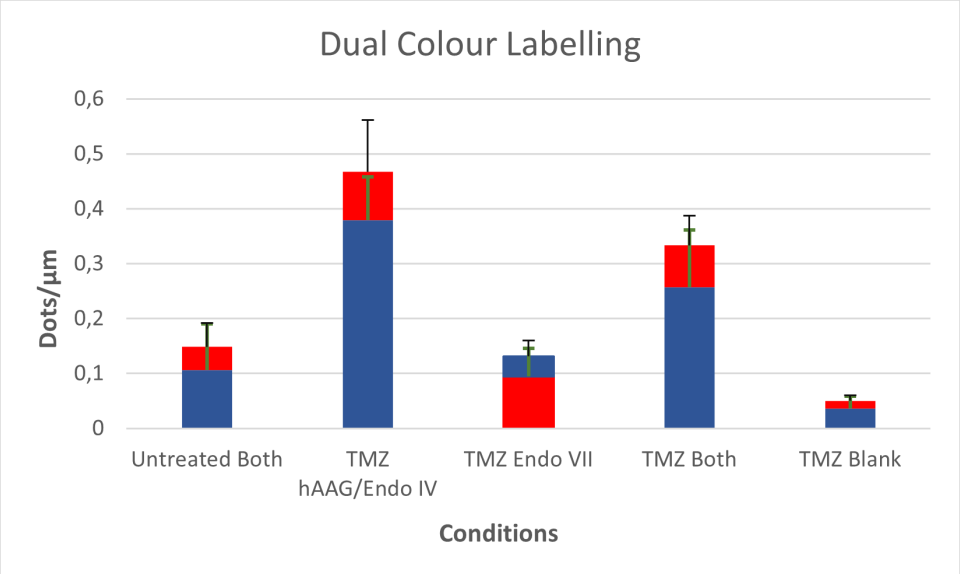

Figure 4.3: Results of one dual colour labelling experiment. Damage displayed as dots per μm DNA. Samples were either labelled using hAAG and Endo IV in the first step, followed by Endo VII in the second step (TMZ Both, Untreated Both), by using hAAG and Endo IV in the first step and no enzyme in the second step (TMZ hAAG/Endo IV), by using Endo VII in the first step and no enzyme in the second step (TMZ Endo VII) or no enzymes in the first or second steps (TMZ Blank). Blue represents repair following addition of hAAG/Endo IV, red represents repair following addition of Endo VII. Error bars represent standard deviation of individual image damage levels as determined by the MATLAB script described in section 3.4.

time of hAAG/Endo IV and compare damage levels to the original one hour incubation time. Nevertheless, the clear decrease in the number of both red and blue dots from their individual use to when excluding all enzymes clearly points to both pathways being utilized in the repair process in vitro. One could therefore reasonably expect an increase in the number of red dots in TMZ both compared to TMZ hAAG/Endo IV and Endo VII, as there would be both residual activity from hAAG/Endo IV and activity from the newly added Endo VII. This is not observed. A continued hAAG/Endo IV activity is therefore alone not a sufficient explanation for the observed results. Given the low specificity of many bacterial enzymes, it is highly possible that there is some overlap in substrate affinity for the hAAG/Endo IV and the Endo VII enzymes. Another possibility is an inhibitory effect when both enzymes are in the same solution.

Also notably in figure 4.3, the number of blue dots per μm is higher for TMZ hAAG/Endo IV than TMZ Both. As they in both cases represent repair from hAAG/Endo IV, one would expect the same level of damage. A similar effect can be observed in figure 4.2a, where all three repeats are included, however the difference is non-significant. This suggests an individual variation for this particular repeat rather than a systematic error.

To assess possible overlap the results displayed in figure 4.2 were replotted as the ratio of blue dots over the total number of dots. When looking at the ratio of the dots, as can be seen in figure 4.4, the difference corresponds to around 3.9 %-units. This is in the expected range of O^6-MeG to the total methylations induced by TMZ. However, the difference is small and non-significant. As such, this is not sufficient evidence to confirm that Endo VII repairs O^6-MeG.

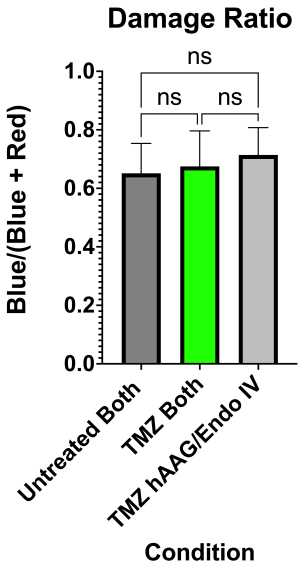

Figure 4.4: Damage ratio calculated as the number of blue dots per μm DNA divided by the total number of dots per μm DNA. Samples were either labelled using hAAG and Endo IV in the first step, followed by Endo VII in the second step (TMZ Both, Untreated Both) or by using hAAG and Endo IV in the first step and no enzyme in the second step (TMZ hAAG/Endo IV). Error bars represent the standard deviation of three repeats.

The possibility of an inhibitory effect was investigated using the single-colour labelling process described in section 3.2.1. DNA was labelled using either only hAAG and Endo IV, only Endo VII or all three enzymes simultaneously. The damage for the enzymes used separately was added together for comparison purposes. The difference between using the enzymes separately and simultaneously was non-significant as shown in figure 4.5. This contradicts the theory of an inhibitory effect when the enzymes are used simultaneously. A more likely theory is therefore that there is an overlap in substrate affinity between the enzymes.
While the knowledge on Endo VII is limited in comparison with that of hAAG and Endo IV, the known substrates of Endo VII can give some suggestions on its effect on DNA treated with TMZ. While Endo VII has been demonstrated to have affinity for mismatches such as G-T, which can result from O^6-MeG, this mispairing is replication dependent. The PBMCs did not undergo a replication process in this study and should therefore not have a notable amount of mispairings. Furthermore, MGMT, which is present in PBMCs[80], can directly repair O^6-MeG, bypassing the need for gap-filling by DNA polymerase. It is therefore possible that O^6-MeG

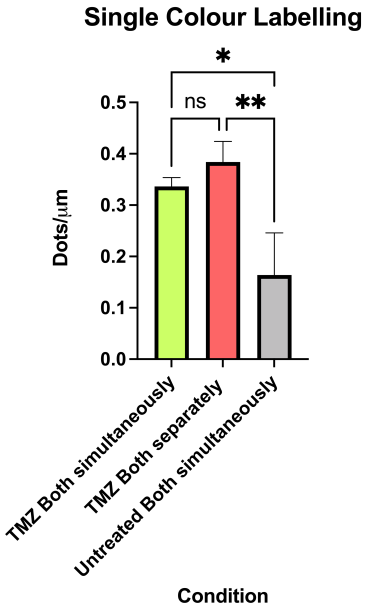

Figure 4.5: Average damage shown as number of ATTO-550 dots per um DNA. Samples were either treated with hAAG, Endo IV and Endo VII simultaneously (TMZ Both simultaneously, Untreated Both simultaneously) or with only hAAG and Endo IV or only Endo VII. The damage for the enzymes used separately was then added together in TMZ Both Separately. Error bars represent the standard deviation of three repeats.

levels are already low when initiating repair and labelling after DNA extraction. This would however need to be confirmed, e.g. by inhibiting MGMT and observing the effect this has on O^6-MeG levels. Especially considering that suppression of MGMT levels have been observed in conjunction with TMZ treatment[81]. O^6-MeG represents a relatively small distortion, and there has been no study that has observed an affinity of Endo VII to O^6-MeG, but it may be possible given the wide substrate range of Endo VII. Another possibility is the repair of crosslinks, which has been reported to be performed by Endo VII[38]. While TMZ itself does not serve as a crosslinking agent, the methyladducts that TMZ induces can lead to crosslinking by formation of AP-sites, which are prone to interstrand crosslinking. Given that these AP-sites can spontaneously occur by N^7-MeG, this could be a potential explanation for the substrate overlap. Furthermore, Endo VII has been reported to have affinity for the AP-sites themselves, strengthening the theory of a substrate overlap. If Endo VII has a slower reaction rate than hAAG/Endo IV, and or a smaller number of lesions to repair (e.g., only AP-sites as opposed to AP-sites and all N^7-MeG and N^3-MeA lesions for hAAG/Endo IV) it could explain why the effect of Endo VII appears to be masked by hAAG/Endo IV activity. Regardless of its substrate, Endo VII clearly has a repairing function on TMZ-treated DNA. The mechanisms of this function remain to be fully elucidated however, for which more research is needed. It is also possible that the low specificity of Endo VII makes it an unsuitable enzyme for this assay. To further investigate this issue, reversing the order in which the enzymes are added could provide useful information. For

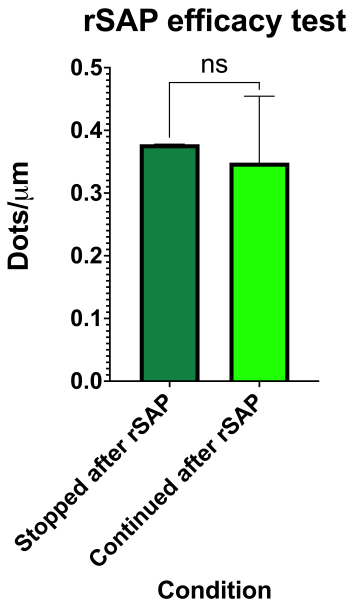

Figure 4.6: Average damage shown as number of ATTO-550 dots per um DNA. Samples were labelled with hAAG and Endo IV. After nucleotide inactivation, the samples were divided in half. For one half, EDTA was added directly (Stopped after rSAP), the other half was left at room temperature for another hour before adding EDTA (Continued after rSAP). Error bars represent the standard deviation of two repeats.

example, a decrease in the number of blue dots would further support the idea of a substrate overlap between the enzymes.
As this thesis was based on the work of Torchinsky et al., it is also of interest to compare results. While Torchinsky et al. noted some substrate overlap with the enzymes used in their paper, the potential residual activity of the enzyme in the first reaction step was not addressed. As they also utilize Endo IV in the first step, one could reasonably expect a similar effect in regard to enzyme activity as for this study. However, as there is no available data on this topic in their paper, it is unknown if they would observe similar issues with how representative colours actually are of enzymatic activity.

4.1.2 rSAP efficacy test

To ensure sufficient nucleotide inactivation of previously added nucleotides was achieved by the addition of rSAP, a separate test was conducted. This test followed the procedure described in section 3.2.2 until after nucleotide inactivation with rSAP. After this, half the sample was inactivated directly with EDTA, the other half was left at room temperature for one hour before deactivating with EDTA. The process was done twice. Figure 4.6 shows the average damage recorded.
This data shows a slight decrease in damage levels following an additional hour of incubation. However, this decrease is non-significant, suggesting rSAP inactivates the free nucleotides remaining in the sample.

4.2 Optimization

This project involved optimization of several aspects of the SMI process. Firstly, relating to the integrity of the acquired blood samples, secondly, regarding the coverslip preparation process, and lastly, the suitability of labelled DNA storage for use in this assay.

4.2.1 Effect of Blood Storage on Basal DNA Damage

The blood samples are delivered in EDTA vials to prevent coagulation. However, this is not equivalent to the environment PBMCs experience in the blood stream, and tests were conducted to assess how this affects the DNA of the PBMCs and how long from the sampling time this effect becomes significant. Three blood storage tests were performed wherein five blood samples were mixed. Average blood sample extraction times are presented in table 4.2.

Table 4.2: Sampling time noted on the blood samples provided by Sahlgrenska University Hospital, rounded to the nearest half hour.

Test iteration	Sampling time
1	5:30
2	7:30
3	5:30

PBMCs were extracted according to section 3.1.1 at different time points where the extraction points are labelled as the time passed since sampling. After extraction there was no cell treatment, and the cells were resuspended and lysed immediately before extracting the DNA according to section 3.1.3. The DNA samples were repaired and labelled and kept at -20 until imaging. The images were analysed using the software described in section 3.4. The calculated DNA damage, in number of dots per um was compiled for each experiment. Figure 4.7 shows all three experiments side by side.
Test 1 and 2 show similar trends, with an increase in damage as time increases. In contrast, test 3 exhibits no linear trend behaviour, with higher damage levels overall and a peak at the mid-point of six hours. Given that five blood samples were used, the different pattern observed for test three is likely not due to variation in blood sample quality. The isolation of DNA from PBMCs is a multistep process, and there are therefore many steps in which the natural imperfections in a researcher's actions may affect the results. Slight variations in the time and intensity at which a sample is vortexed could for example have an effect. There could also be slight variations in concentrations of different components in the sample that have an effect. As the irregular results are likely due to human error, test 3 was excluded from the analysis. It must then be mentioned that for time points 2, 8 and 10, there was only one available value due to different times of blood drawal for the provided samples. To facilitate calculation of statistical significance, single values were grouped together with the closest time point. The 2 hour value was grouped together with the 4 hour values. The values at 8 and 10 hours were also grouped together (denoted 8 hours).

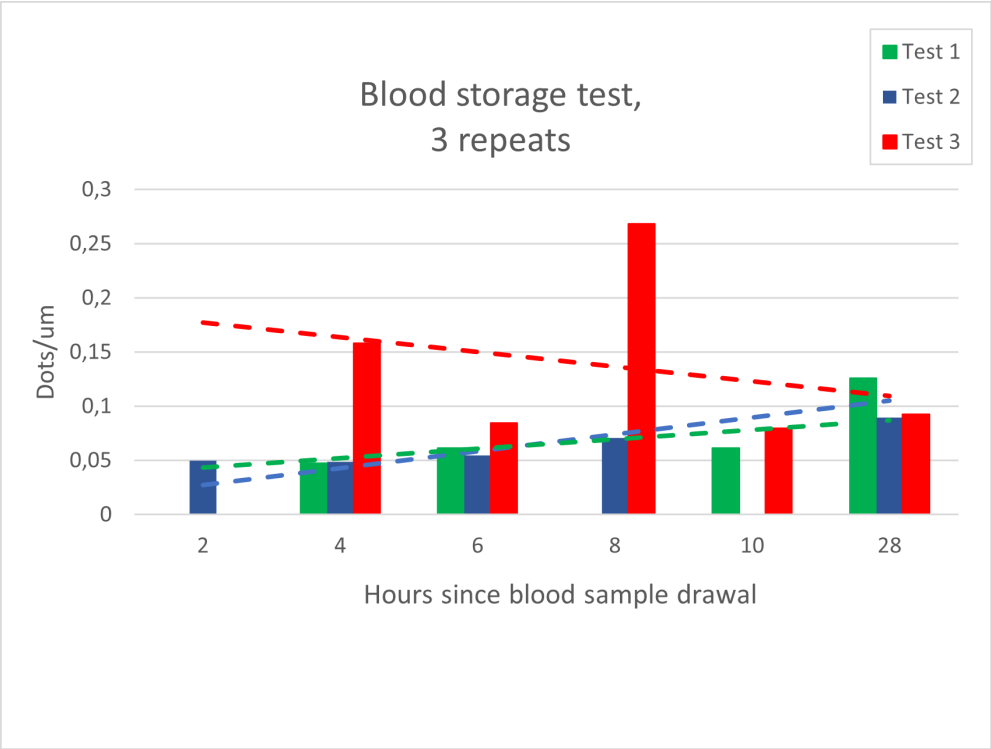

Figure 4.7: Damage levels as represented by number of dots per um DNA, plotted against time since blood sampling. The different colours of the bars represent the test iteration. A linear regression was performed for each iteration to observe potential trends. For tests 1 and 2, the linear regressions have positive slopes, for test 3 the slope is negative.

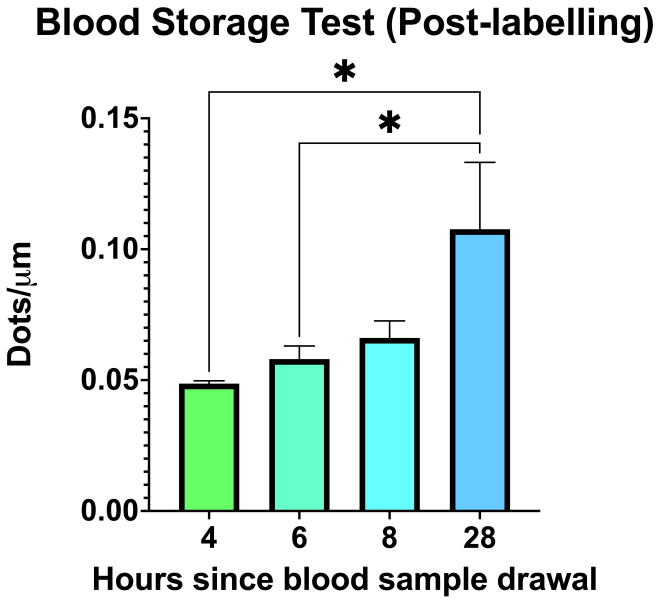

Figure 4.8: Mean data from two blood storage tests. DNA was extracted from blood at regular intervals. The extracted DNA was repaired using an enzyme cocktail and imaged. The images were analyzed for number of dUTP-ATTO-550 dots per strand. Error bars represent the standard deviation of two to three values.

Figure 4.8 shows the average damage recorded in test 1 and 2, together with the statistical significance of the results.
While there is a slight trend toward increase in damage levels with time, this was non-significant for the DNA extracted on the same day as the blood samples where drawn. In particular, damage after 28 hours is significantly higher than at 4 and 6 hours. These results suggest an increase in basal DNA damage with time, but likely a negligible difference if blood samples are used on the same day they are drawn.

4.2.2 Coverslip Silanization Time Test

The APTES/ATMS solution was prepared as described in 3.3.1. At 30 minute intervals, coverslips were removed and used to image Lambda or human DNA. The DNA molecules were counted and measured using the available software. The results are displayed in figure 4.9 where figure 4.9a shows the results from tests with bacterial DNA and figure 4.9b shows the results from the human DNA test.
From this figure there appears to be no clear trend in how coverslip submersion between 30 minutes and 2 hours affects the stretching of DNA. The accuracy of these average lengths must however be discussed. To prevent the software from recognizing background as DNA strands, a minimum strand length must be set, in this case at 5.5 μm. Thus, an important part of the picture, i.e. the percentage of DNA stretched, is unavailable as highly coiled DNA is not included in the calculations. This may lead to misrepresentation of the true sample. Furthermore, due to variations in intensity along strands, some strands were recognized as two strands rather than one by the MATLAB code, further increasing the uncertainty of the results. To

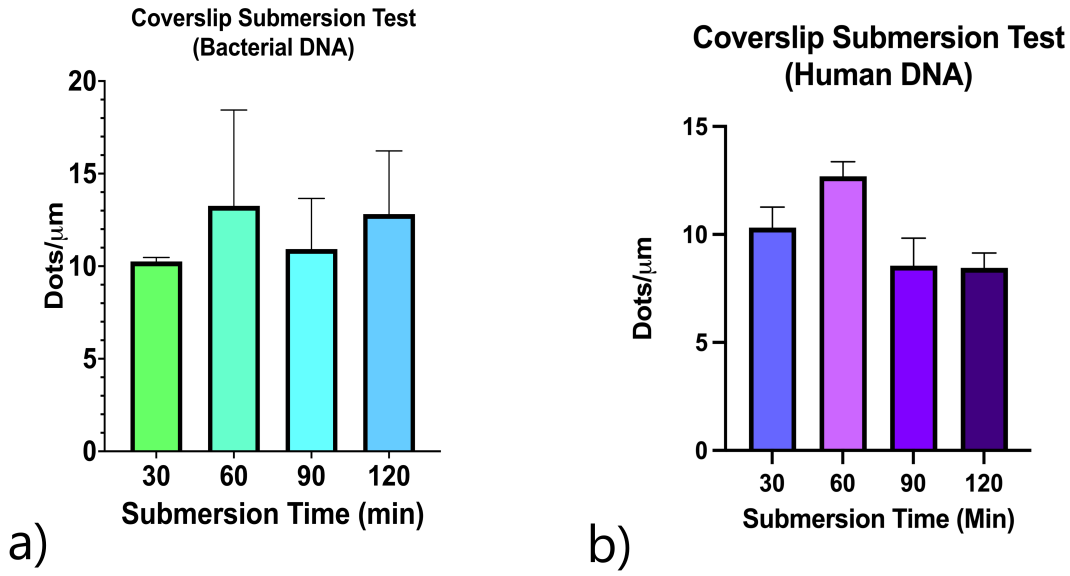

Figure 4.9: DNA strand length as a function of coverslip submersion time. a) Shows the average of two repeats using Lambda DNA (NEB). Error bars represent the standard deviation of two repeats. b) Shows one experiment using human DNA. Error bars represent standard deviation of individual image damage levels as determined by the MATLAB script described in section 3.4.

complement this data, a visual inspection was therefore also necessary. Figure 4.10 shows snapshots from the first iteration of this test of Lambda DNA stretched at different coverslip submersion times.
From the images in figure 4.10, there appears to be no clear trend in quality between time points. In all cases, there are areas of the coverslip when the DNA is highly stretched and areas where it is less so. While it is difficult to draw a definitive conclusion with the data available, the suggestion is that 30 minutes of submersion in the APTES/ATMS/acetone solution could be sufficient.

4.2.3 Effect of Storage Time and Temperature of Labelled DNA on Measured DNA Damage

To evaluate the effect storing labelled DNA has on observed DNA damage levels, two samples from the second blood storage test were used. Samples were re-imaged the day after, three days after and one week after the initial imaging. Setting the first imaging as day 1, this gave data points for days 2, 4 and 8. Samples were kept both at 4 and -20 °C for comparison. Due to differences in initial damage levels for the two samples, results were divided by the damage recorded on the first day of imaging. This converts the quantified damage into relative numbers, i.e., how much damage has increased or decreased over time. The two samples were then averaged

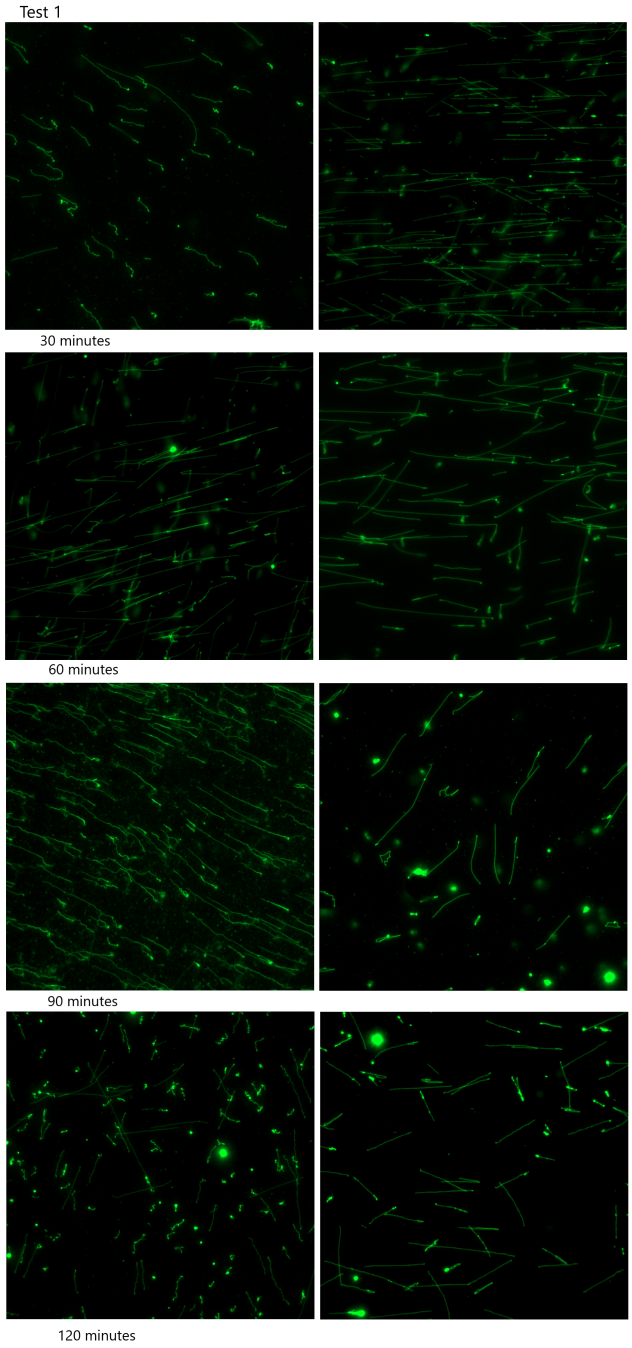

Figure 4.10: Stretched Lambda DNA strands stained with YOYO-1 dye. Images were taken using coverslips with different silanization time. Two images per time point are shown.

and plotted, as seen in figure 4.11.

For day 8, only data from samples stored at -20 °C is available. Upon trying to image the day 8 4 °C samples the DNA was either unable to stretch and/or highly fragmented. The damage recorded on day 4 is also significantly higher than the original damage for the 4 °C samples, further suggesting that 4 °C is not a suitable temperature for long-time storage. There is some variation in damage levels when

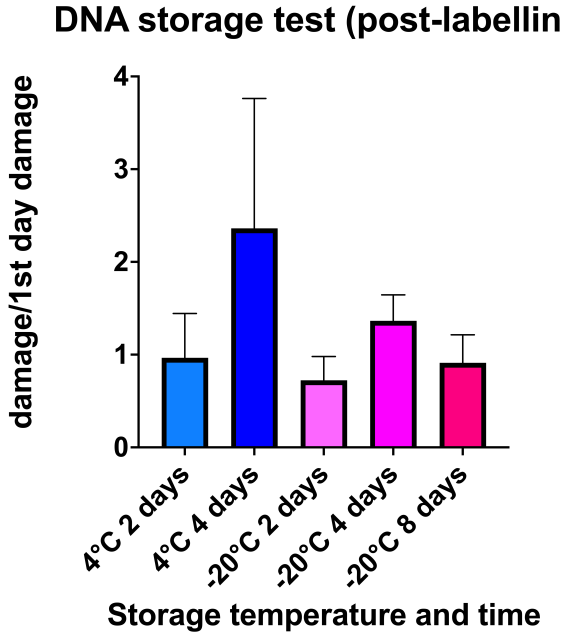

Figure 4.11: Recorded dots per μm for different days of imaging divided by initially measured dots per μm. Samples were stored either at 4°C or -20°C. There is no data point for day 8 for samples kept at 4°C. Error bars represent standard deviation of two repeats, except for '-20 °C 4 days' as this sample only has one available value. The standard deviation was instead set as the mean standard deviation of the two other -20 °C samples.

storing samples at -20 °C although not as drastic as for 4 °C storage. It must also be mentioned that only one of the -20 °C samples was imaged on day 4 due to limited time. While this experiment ought to be repeated to acquire more data points, the results suggest that storing labelled DNA at 4 °C for a longer period of time is not suitable. In particular, repeating the experiment with DNA treated with, e.g., TMZ would be valuable, as the added damage might affect the results.

5
Conclusion

DNA exposed to the chemotherapeutic drug TMZ was successfully labelled using two spectrally distinct fluorescent nucleotides, and two different sets of repair enzymes, hAAG/Endo IV and Endo VII. Verification tests suggest either an overlap in substrate affinity or a continued activity of hAAG/Endo IV after one hour of incubation. Despite the overlap, results from repairing with the enzymes separately indicate activity from both, albeit much lower for Endo VII.
One limit of this study is how representative the enzymes used are of those involved during cellular DNA repair. In particular, the enzyme mainly involved in repairing O^6-MeG, MGMT, cannot be used for this assay as it reverses the methylation without base or nucleotide excision, preventing labelling of O^6-MeG sites. As PBMCs express MGMT, although at highly variable levels, it is even possible that the induced O^6-MeG is largely repaired before DNA extraction takes place. While the MMR pathway may be a possible substitute due to the mispairing of O^6-MeG with thymine, the assay did not include a cell replication process. When hAAG/Endo IV is absent, Endo VII clearly repairs damage on TMZ treated DNA strands, but the specific damage it repairs cannot be fully determined from the results in this study. From the wide range of substrates that have been reported for Endo VII, the most likely is perhaps the AP-sites that form by spontaneous or enzymatic depurination of N^7-MeG and/or the interstrand crosslinks derived from these AP-sites.
While it is difficult to draw conclusions regarding the effect of Endo VII, the effect of the well-characterized hAAG/Endo IV enzymes is easier to interpret. By comparing the results for the different conditions in figures 4.2a, 4.2b, and 4.1, one can see that hAAG/Endo IV have a large impact on the repair process. Given that the substrates for these enzymes are known, and that rSAP was shown to be effective, one can reasonably assume that the blue dots to a high degree represent the activity of hAAG and Endo IV. It can also be concluded that 1 hour of incubation is not sufficient for hAAG/Endo IV to repair all lesions for samples treated with 800 μm TMZ. For future work, studying the effect of an increased incubation time would be highly useful.

In addition to the conclusions regarding simultaneous detection of different lesion types, some indications for future work with the general assay could be obtained. Particularly two factors are of note to preserve sample quality. Firstly, when using PBMCs for this assay, DNA should be isolated on the same day as the blood samples were drawn to minimize confounding factors. Secondly, that two hours of coverslip silanization when using the protocol in this paper is not necessary. Lastly, storing labelled DNA at 4 °C for a longer period is not recommended.

References

[1] Socialstyrelsen. Statistik om Dödsorsaker år 2020. 2021. Available from: https://www.socialstyrelsen.se/publikationer/.

[2] Gao Q, Zhou G, Lin SJ, Paus R, Yue Z. How chemotherapy and radiotherapy damage the tissue: comparative biology lessons from feather and hair models. Experimental dermatology. 2019;28(4):413–418. Available from: https://doi.org/10.1111/exd.13846.

[3] Blom K, Nygren P, Larsson R, Andersson CR. Predictive value of ex vivo chemosensitivity assays for individualized cancer chemotherapy: a meta-analysis. SLAS TECHNOLOGY: Translating Life Sciences Innovation. 2017;22(3):306–314. Available from: https://doi.org/10.1177/2472630316686297.

[4] Hoffman RM. In vitro assays for chemotherapy sensitivity. Critical reviews in oncology/hematology. 1993;15(2):99–111. Available from: https://doi.org/10.1016/1040-8428(93)90050-E.

[5] Zhang J, Stevens MF, Bradshaw TD. Temozolomide: mechanisms of action, repair and resistance. Current molecular pharmacology. 2012;5(1):102–114. Available from: https://doi.org/10.2174/1874467211205010102.

[6] Sánchez-Suárez P, Ostrosky-Wegman P, Gallegos-Hernández F, Peñarroja-Flores R, Toledo-García J, Bravo JL, et al. DNA damage in peripheral blood lymphocytes in patients during combined chemotherapy for breast cancer. Mutation Research/Fundamental and Molecular Mechanisms of Mutagenesis. 2008;640(1-2):8–15. Available from: https://doi.org/10.1016/j.mrfmmm.2007.11.008.

[7] Krynetskiy E, Krynetskaia N, Rihawi D, Wieczerzak K, Ciummo V, Walker E. Establishing a model for assessing DNA damage in murine brain cells as a molecular marker of chemotherapy-associated cognitive impairment. Life sciences. 2013;93(17):605–610. Available from: https://doi.org/10.1016/j.lfs.2013.03.013.

[8] Ji J, Zhang Y, Redon CE, Reinhold WC, Chen AP, Fogli LK, et al. Phosphorylated fraction of H2AX as a measurement for DNA damage in cancer cells and potential applications of a novel assay. PloS one. 2017;12(2):e0171582. Available from: https://doi.org/10.1371/journal.pone.0171582.

[9] Erhola M, Toyokuni S, Okada K, Tanaka T, Hiai H, Ochi H, et al. Biomarker

evidence of DNA oxidation in lung cancer patients: association of urinary 8-hydroxy-2-deoxyguanosine excretion with radiotherapy, chemotherapy, and response to treatment. FEBS letters. 1997;409(2):287–291. Available from: https://doi.org/10.1016/S0014-5793(97)00523-1.

[10] Krynetskaia NF, Phadke MS, Jadhav SH, Krynetskiy EY. Chromatin-associated proteins HMGB1/2 and PDIA3 trigger cellular response to chemotherapy-induced DNA damage. Molecular cancer therapeutics. 2009;8(4):864–872. Available from: https://doi.org/10.1158/1535-7163.MCT-08-0695.

[11] Wu Z, Lee S, Qiao Y, Li Z, Lee P, Lee Y, et al. Polycomb protein EZH2 regulates cancer cell fate decision in response to DNA damage. Cell Death & Differentiation. 2011;18(11):1771–1779. Available from: https://doi.org/10.1038/cdd.2011.48.

[12] Singh V, Johansson P, Lin YL, Hammarsten O, Westerlund F. Shining light on single-strand lesions caused by the chemotherapy drug bleomycin. DNA repair. 2021;105:103153. Available from: https://doi.org/10.1016/j.dnarep.2021.103153.

[13] Lee J, Park HS, Lim S, Jo K. Visualization of UV-induced damage on single DNA molecules. Chemical Communications. 2013;49(42):4740–4742. Available from: https://doi.org/10.1039/C3CC38884K.

[14] Torchinsky D, Michaeli Y, Gassman NR, Ebenstein Y. Simultaneous detection of multiple DNA damage types by multi-colour fluorescent labelling. Chemical Communications. 2019;55(76):11414–11417. Available from: https://doi.org/10.1039/C9CC05198H.

[15] Preston BD, Albertson TM, Herr AJ. DNA replication fidelity and cancer. In: Seminars in cancer biology. vol. 20. Elsevier; 2010. p. 281–293. Available from: https://doi.org/10.1016/j.semcancer.2010.10.009.

[16] Chatterjee N, Walker GC. Mechanisms of DNA damage, repair, and mutagenesis. Environmental and molecular mutagenesis. 2017;58(5):235–263. Available from: https://doi.org/10.1002/em.22087.

[17] Martincorena I, Campbell PJ. Somatic mutation in cancer and normal cells. Science. 2015;349(6255):1483–1489. Available from: https://doi.org/10.1126/science.aab4082.

[18] Stratton MR, Campbell PJ, Futreal PA. The cancer genome. Nature. 2009;458(7239):719–724. Available from: https://doi.org/10.1038/nature07943.

[19] Gao M, Zhou H, Skolnick J. Insights into disease-associated mutations in the human proteome through protein structural analysis. Structure. 2015;23(7):1362–1369. Available from: https://doi.org/10.1016/j.str.2015.03.028.

[20] Scull CM, Tabas I. Mechanisms of ER stress-induced apoptosis in atherosclero-

sis. Arteriosclerosis, thrombosis, and vascular biology. 2011;31(12):2792–2797. Available from: https://doi.org/10.1161/ATVBAHA.111.224881.

[21] Roos WP, Kaina B. DNA damage-induced cell death by apoptosis. Trends in molecular medicine. 2006;12(9):440–450. Available from: https://doi.org/10.1016/j.molmed.2006.07.007.

[22] Moore LD, Le T, Fan G. DNA methylation and its basic function. Neuropsychopharmacology. 2013;38(1):23–38. Available from: https://doi.org/10.1038/npp.2012.112.

[23] Das PM, Singal R. DNA methylation and cancer. Journal of clinical oncology. 2004;22(22):4632–4642. Available from: https://doi.org/10.1200/JCO.2004.07.151.

[24] Gates KS, Nooner T, Dutta S. Biologically relevant chemical reactions of N7-alkylguanine residues in DNA. Chemical research in toxicology. 2004;17(7):839–856. Available from: https://doi.org/10.1021/tx049965c.

[25] Lindahl T. Instability and decay of the primary structure of DNA. nature. 1993;362(6422):709–715. Available from: https://doi.org/10.1038/362709a0.

[26] Bignami M, O'Driscoll M, Aquilina G, Karran P. Unmasking a killer: DNA O6-methylguanine and the cytotoxicity of methylating agents. Mutation Research/Reviews in Mutation Research. 2000;462(2-3):71–82. Available from: https://doi.org/10.1016/S1383-5742(00)00016-8.

[27] Pastink A, Eeken JC, Lohman PH. Genomic integrity and the repair of double-strand DNA breaks. Mutation Research/Fundamental and Molecular Mechanisms of Mutagenesis. 2001;480:37–50. Available from: https://doi.org/10.1016/S0027-5107(01)00167-1.

[28] Osawa T, Davies D, Hartley J. Mechanism of cell death resulting from DNA interstrand cross-linking in mammalian cells. Cell death & disease. 2011;2(8):e187–e187. Available from: https://doi.org/10.1038/cddis.2011.70.

[29] Strobel H, Baisch T, Fitzel R, Schilberg K, Siegelin MD, Karpel-Massler G, et al. Temozolomide and other alkylating agents in glioblastoma therapy. Biomedicines. 2019;7(3):69. Available from: https://doi.org/10.3390/biomedicines7030069.

[30] Dutta S, Chowdhury G, Gates KS. Interstrand cross-links generated by abasic sites in duplex DNA. Journal of the American Chemical Society. 2007;129(7):1852–1853. Available from: https://doi.org/10.1021/ja067294u.

[31] Krokan HE, Bjørås M. Base excision repair. Cold Spring Harbor perspectives in biology. 2013;5(4). Available from: https://doi.org/10.1101/cshperspect.a012583.

[32] Kondo N, Takahashi A, Ono K, Ohnishi T. DNA damage induced by alkylating agents and repair pathways. Journal of nucleic acids. 2010;2010. Available from: https://doi.org/10.4061/2010/543531.

[33] Wyatt MD, Pittman DL. Methylating agents and DNA repair responses: Methylated bases and sources of strand breaks. Chemical research in toxicology. 2006;19(12):1580–1594. Available from: https://doi.org/10.1021/tx060164e.

[34] Robertson A, Klungland A, Rognes T, Leiros I. DNA repair in mammalian cells. Cellular and molecular life sciences. 2009;66(6):981–993. Available from: https://doi.org/10.1007/s00018-009-8736-z.

[35] Wood RD, Mitchell M, Sgouros J, Lindahl T. Human DNA repair genes. Science. 2001;291(5507):1284–1289. Available from: https://doi.org/10.1126/science.1056154.

[36] Solaro PC, Birkenkamp K, Pfeiffer P, Kemper B. Endonuclease VII of phage T4 triggers mismatch correction in vitro. Journal of molecular biology. 1993;230(3):868–877. Available from: https://doi.org/10.1006/jmbi.1993.1207.

[37] Mizuuchi K, Kemper B, Hays J, Weisberg RA. T4 endonuclease VII cleaves Holliday structures. Cell. 1982;29(2):357–365. Available from: https://doi.org/10.1016/0092-8674(82)90152-0.

[38] Kasparkova J, Brabec V. Recognition of DNA interstrand cross-links of cis-diamminedichloroplatinum (II) and its trans isomer by DNA-binding proteins. Biochemistry. 1995;34(38):12379–12387. Available from: https://doi.org/10.1021/bi00038a035.

[39] Greger B, Kemper B. An apyrimidinic site kinks DNA and triggers incision by endonuclease VII of phage T4. Nucleic Acids Research. 1998 10;26(19):4432–4438. Available from: https://doi.org/10.1093/nar/26.19.4432.

[40] Gillet LC, Schärer OD. Molecular mechanisms of mammalian global genome nucleotide excision repair. Chemical reviews. 2006;106(2):253–276. Available from: https://doi.org/10.1021/cr040483f.

[41] Plosky B, Samson L, Engelward BP, Gold B, Schlaen B, Millas T, et al. Base excision repair and nucleotide excision repair contribute to the removal of N-methylpurines from active genes. DNA repair. 2002;1(8):683–696. Available from: https://doi.org/10.1016/S1568-7864(02)00075-7.

[42] Xiao W, Chow BL. Synergism between yeast nucleotide and base excision repair pathways in the protection against DNA methylation damage. Current genetics. 1998;33(2):92–99. Available from: https://doi.org/10.1007/s002940050313.

[43] Li X, Heyer WD. Homologous recombination in DNA repair and DNA damage tolerance. Cell research. 2008;18(1):99–113. Available from: https://doi.org/10.1038/cr.2008.1.

[44] Chang HH, Pannunzio NR, Adachi N, Lieber MR. Non-homologous DNA end joining and alternative pathways to double-strand break repair. Nature reviews Molecular cell biology. 2017;18(8):495–506. Available from: https://doi.org/10.1038/nrm.2017.48.

[45] Woodbine L, Gennery AR, Jeggo PA. The clinical impact of deficiency in DNA non-homologous end-joining. DNA repair. 2014;16:84–96. Available from: https://doi.org/10.1016/j.dnarep.2014.02.011.

[46] Eker A, Quayle C, Chaves I, Van der Horst G. DNA repair in mammalian cells. Cellular and molecular life sciences. 2009;66(6):968–980. Available from: https://doi.org/10.1007/s00018-009-8735-0.

[47] Pitot HC. The molecular biology of carcinogenesis. Cancer. 1993;72(S3):962–970. Available from: https://doi.org/10.1002/1097-0142(19930801)72:3+<962::AID-CNCR2820721303>3.0.CO;2-H.

[48] Croce CM. Oncogenes and cancer. New England journal of medicine. 2008;358(5):502–511. Available from: https://doi.org/10.1056/NEJMra072367.

[49] Payne SR, Kemp CJ. Tumor suppressor genetics. Carcinogenesis. 2005;26(12):2031–2045. Available from: https://doi.org/10.1093/carcin/bgi223.

[50] Hanahan D, Weinberg RA. The hallmarks of cancer. cell. 2000;100(1):57–70. Available from: https://doi.org/10.1016/S0092-8674(00)81683-9.

[51] Goldie JH. Drug resistance in cancer: a perspective. Cancer and Metastasis Reviews. 2001;20(1):63–68. Available from: https://doi.org/10.1023/a:1013164609041.

[52] Cairns RA, Harris IS, Mak TW. Regulation of cancer cell metabolism. Nature Reviews Cancer. 2011;11(2):85–95. Available from: https://doi.org/10.1038/nrc2981.

[53] Hashida M. Advocation and advancements of EPR effect theory in drug delivery science: A commentary. Elsevier; 2022. Available from: https://doi.org/10.1016/j.jconrel.2022.04.031.

[54] Nia HT, Munn LL, Jain RK. Physical traits of cancer. Science. 2020;370(6516). Available from: https://doi.org/10.1126/science.aaz0868.

[55] Chu E, Sartorelli A. Cancer chemotherapy. Lange's Basic and Clinical Pharmacology,. 2018:948–976.

[56] De Vries NA, Beijnen JH, Boogerd W, Van Tellingen O. Blood–brain barrier and chemotherapeutic treatment of brain tumors. Expert review of neurotherapeutics. 2006;6(8):1199–1209. Available from: https://doi.org/10.1586/14737175.6.8.1199.

[57] Nygren P. What is cancer chemotherapy? Acta Oncologica. 2001;40(2-3):166–174. Available from: https://doi.org/10.1080/02841860151116204.

[58] Darkes M, Plosker G, Jarvis B. Temozolomide. American Journal of Cancer. 2002 01;1. Available from: https://doi.org/10.2165/00024669-200201010-00006.

[59] Moerner WE. New directions in single-molecule imaging and analysis. Proceedings of the National Academy of Sciences. 2007;104(31):12596–12602. Available from: https://doi.org/10.1073/pnas.0610081104.

[60] Takahashi S, Oshige M, Katsura S. DNA manipulation and single-molecule imaging. Molecules. 2021;26(4):1050. Available from: https://doi.org/10.3390/molecules26041050.

[61] Carré A, Lacarrière V, Birch W. Molecular interactions between DNA and an aminated glass substrate. Journal of colloid and interface science. 2003;260(1):49–55. Available from: https://doi.org/10.1016/S0021-9797(02)00147-9.

[62] Labit H, Goldar A, Guilbaud G, Douarche C, Hyrien O, Marheineke K. A simple and optimized method of producing silanized surfaces for FISH and replication mapping on combed DNA fibers. BioTechniques. 2008;45(6):649–658. Available from: https://doi.org/10.2144/000113002.

[63] Singh V, Johansson P, Torchinsky D, Lin YL, Öz R, Ebenstein Y, et al. Quantifying DNA damage induced by ionizing radiation and hyperthermia using single DNA molecule imaging. Translational oncology. 2020;13(10):100822. Available from: https://doi.org/10.1016/j.tranon.2020.100822.

[64] Zirkin S, Fishman S, Sharim H, Michaeli Y, Don J, Ebenstein Y. Lighting up individual DNA damage sites by in vitro repair synthesis. Journal of the American Chemical Society. 2014;136(21):7771–7776. Available from: https://doi.org/10.1021/ja503677n.

[65] Collins AR. The comet assay for DNA damage and repair. Molecular biotechnology. 2004;26(3):249–261. Available from: https://doi.org/10.1385/MB:26:3:249.

[66] Boguszewska K, Szewczuk M, Urbaniak S, Karwowski BT. Review:immunoassays in DNA damage and instability detection. Cellular and Molecular Life Sciences. 2019;76(23):4689–4704. Available from: https://10.1007/s00018-019-03239-6.

[67] Figueroa-González G, Pérez-Plasencia C. Strategies for the evaluation of DNA damage and repair mechanisms in cancer. Oncology letters. 2017;13(6):3982–3988. Available from: https://doi.org/10.3892/ol.2017.6002.

[68] Chang CC, Lin CC, Hsieh WL, Lai HW, Tsai CH, Cheng YW. MicroRNA expression profiling in PBMCs: a potential diagnostic biomarker of chronic hepatitis C. Disease markers. 2014;2014. Available from: https://doi.org/10.1155/2014/367157.

[69] Castaldo I, De Rosa M, Romano A, Zuchegna C, Squitieri F, Mechelli R, et al. DNA damage signatures in peripheral blood cells as biomarkers in prodromal

huntington disease. Annals of neurology. 2019;85(2):296–301. Available from: https://doi.org/10.1002/ana.25393.

[70] Nardo G, Pozzi S, Pignataro M, Lauranzano E, Spano G, Garbelli S, et al. Amyotrophic lateral sclerosis multiprotein biomarkers in peripheral blood mononuclear cells. PloS one. 2011;6(10). Available from: https://doi.org/10.1371/journal.pone.0025545.

[71] Mosallaei M, Ehtesham N, Rahimirad S, Saghi M, Vatandoost N, Khosravi S. PBMCs: A new source of diagnostic and prognostic biomarkers. Archives of Physiology and Biochemistry. 2020:1–7. Available from: https://doi.org/10.1080/13813455.2020.1752257.

[72] Corkum CP, Ings DP, Burgess C, Karwowska S, Kroll W, Michalak TI. Immune cell subsets and their gene expression profiles from human PBMC isolated by Vacutainer Cell Preparation Tube (CPT™) and standard density gradient. BMC immunology. 2015;16(1):1–18. Available from: https://doi.org/10.1186/s12865-015-0113-0.

[73] Betsou F, Gaignaux A, Ammerlaan W, Norris PJ, Stone M. Biospecimen science of blood for peripheral blood mononuclear cell (PBMC) functional applications. Current Pathobiology Reports. 2019;7(2):17–27. Available from: https://doi.org/10.1007/s40139-019-00192-8.

[74] Autissier P, Soulas C, Burdo TH, Williams KC. Evaluation of a 12-color flow cytometry panel to study lymphocyte, monocyte, and dendritic cell subsets in humans. Cytometry Part A: The Journal of the International Society for Advancement of Cytometry. 2010;77(5):410–419. Available from: https://doi.org/10.1002/cyto.a.20859.

[75] Friso S, Udali S, Guarini P, Pellegrini C, Pattini P, Moruzzi S, et al. Global DNA hypomethylation in peripheral blood mononuclear cells as a biomarker of cancer risk. Cancer Epidemiology and Prevention Biomarkers. 2013;22(3):348–355. Available from: https://doi.org/10.1158/1055-9965.EPI-12-0859.

[76] Burczynski ME, Twine NC, Dukart G, Marshall B, Hidalgo M, Stadler WM, et al. Transcriptional profiles in peripheral blood mononuclear cells prognostic of clinical outcomes in patients with advanced renal cell carcinoma. Clinical cancer research. 2005;11(3):1181–1189. Available from: https://doi.org/10.1158/1078-0432.1181.11.3.

[77] Ma J, Lin Y, Zhan M, Mann DL, Stass SA, Jiang F. Differential miRNA expressions in peripheral blood mononuclear cells for diagnosis of lung cancer. Laboratory Investigation. 2015;95(10):1197–1206. Available from: https://doi.org/10.1038/labinvest.2015.88.

[78] Ern Ang J, Kaye S, Banerji U. Tissue-based approaches to study pharmacodynamic endpoints in early phase oncology clinical trials. Current drug targets. 2012;13(12):1525–1534. Available from: https://doi.org/10.2174/138945012803530062.

[79] Sengupta S, Marrinan J, Frishman C, Sampath P. Impact of temozolomide on immune response during malignant glioma chemotherapy. Clinical and Developmental Immunology. 2012;2012. Available from: https://doi.org/10.1155/2012/831090.

[80] Janssen K, Eichhorn-Grombacher U, Schlink K, Nitzsche S, Oesch F, Kaina B. Long-time expression of DNA repair enzymes MGMT and APE in human peripheral blood mononuclear cells. Archives of toxicology. 2001;75(5):306–312. Available from: https://doi.org/10.1007/s002040100226.

[81] Gander M, Decosterd L, Bonfanti M, Marzolini C, Shen F, Liénard D, et al. Sequential administration of temozolomide and fotemustine: depletion of O6-alkyl guanine-DNA transferase in blood lymphocytes and in tumours. Annals of Oncology. 1999;10(7):831–838. Available from: https://doi.org/10.1023/A:1008304032421.

A

Appendix

A.1 MATLAB script for DNA damage quantification settings

Table A.1 shows the settings used for the MATLAB script provided by the department of Astronomy and Theoretical Physics at the University of Lund. An EdgeScore is assigned a detected molecule. Any molecule with a lower log(EdgeScore) than the minimum is rejected. A molecule with a higher length than the maximum or a lower length than the minimum is rejected. A DotScore is assigned a detected dot. Any dot with a lower DotScore than the minimum, or not located on a detected molecule is rejected. A dot with a width higher than maximum or lower than minimum is rejected. A dot with a shorter distance to the detected edge of a molecule than the Edge margin is rejected. Molecule eccentricity refers to the ratio between the distance of the long edge ends to the center of the molecule and the distance of the short edge ends to the center of the molecule. The molecule-to-convex-hull ratio refers to the ratio between the molecule area and that of the smallest possible area convex polygon enclosing the molecule.

Table A.1: Settings used when running the MATLAB scrip for recognition of DNA molecules and dots.

Variable	**Value or setting**
Width of LoG filter (nm)	300
Minimum log(EdgeScore)	Auto
Minimum DotScore	Variable
Minimum Width (pixels)	1
Maximum Width (pixels)	Infinite
Minimum Length (pixels)	50
Maximum Length (pixels)	Infinite
Edge margin (pixels)	2
Minimum molecule eccentricity	0.8
Minimum molecule-to-convex-hull ratio	0.6

A.2 p-values

The p-values calculated for the obtained data are presented in tables according to their respective experiment. Table A.2 shows the p-values calculated with a one-way ANOVA for samples labelled with the dual colour assay method, corresponding to figure 4.2.

Table A.2: p-values for the dual colour labelling tests.

Comparison	p-value hAAG/Endo IV dots	p-value Endo VII dots
TMZ Both vs. TMZ hAAG Endo IV	0.7621	0.8188
TMZ Both Untreated Both	0.0121	0.0667
TMZ hAAG/Endo IV Untreated Both	0.0058	0.1453

Table A.3 shows the p-values calculated with a one-way ANOVA for the ratios from the values dual colour labelling samples. The ratios are shown in figure 4.4. Table

Table A.3: p-values for the ratios calculated from the dual colour labelling tests.

Comparison	p-value
TMZ Both vs. TMZ hAAG Endo IV	0.8955
TMZ Both vs. Untreated Both	0.9603
TMZ hAAG/Endo IV vs. Untreated Both	0.7593

A.4 shows the p-values calculated with a one-way ANOVA for the single colour labelling samples displayed in figure 4.5.

Table A.4: p-values for the single colour labelling tests.

Comparison	p-value
TMZ Both Simultaneously vs. TMZ Both Separately	0.5527
TMZ Both Simultaneously vs. Untreated Both Simultaneously	0.0180
TMZ Both Separately vs. Untreated Both Simultaneously	0.0057

Table A.5 shows the p-values calculated with an unpaired t-test for the rSAP efficiency test displayed in figure 4.6.

Table A.5: p-values for the rSAP efficiency test.

Comparison	p-value
Stopped after rSAP vs. Continued after rSAP	0.7342

Table A.6 shows the p-values calculated with a one-way ANOVA for the tests regarding the effect of blood storage on basal DNA damage, corresponding to figure 4.8.

Table A.6: p-values for the tests on the effect of blood storage on basal DNA damage

Comparison	p-value
4 hours vs 6 hours	0.8270
4 hours vs 8 hours	0.4591
4 hours vs 28 hours	0.0112
6 hours vs 8 hours	0.9041
6 hours vs 28 hours	0.0328
8 hours vs 28 hours	0.0630

DEPARTMENT OF BIOLOGY AND BIOLOGICAL ENGINEERING
CHALMERS UNIVERSITY OF TECHNOLOGY
Gothenburg, Sweden
www.chalmers.se

CHALMERS
UNIVERSITY OF TECHNOLOGY